Sensitivity of paleonutrient tracer distributions and deep-sea circulation to glacial boundary conditions

A. Winguth, D. Archer, J.-C. Duplessy, E. Maier-Reimer, U. Mikolajewicz

PALEOCEANOGRAPHY, VOL. 14, NO. 3, PAGES 304-323, JUNE 1999

Sensitivity of paleonutrient tracer distributions and deep-sea circulation to glacial boundary conditions

A. M. E. Winguth and D. Archer

Department of Geophysical Sciences, University of Chicago, Chicago, Illinois

J.-C. Duplessy

Centre des Faibles Radioactivites Laboratoire mixte CNRS-CEA, Gif sur Yvette, France

E. Maier-Reimer and U. Mikolajewicz

Max-Planck-Institut für Meteorologie, Hamburg, Germany

Abstract. We use a carbon cycle model coupled to an ocean general circulation model to explore the links between sea surface boundary conditions, the deep-sea circulation, and the distribution of paleonutrient tracers ($\delta^{13}C$ and Cd/Ca) from Last Glacial Maximum (21,000 B.P.) sediments. A glacial flow field with a shallower and 50% reduced North Atlantic overturning circulation generally reproduces the tracer data but cannot explain the strong glacial-interglacial shift in $\delta^{13}C$ in the Southern Ocean. Sensitivity experiments with changes of ± 1 in salinity in the glacial salinity boundary fields show circulation patterns ranging from even stronger than the present day one to nearly a shutdown of the Atlantic deep-sea circulation. Our model results indicate that the overturning in the North Atlantic is linearly related to the zonal wind forcing in the Southern Ocean but with half of the sensitivity of *Toggweiler and Samuels* [1993]. Atmospheric pCO_2 appears to be insensitive to changing circulation and sea surface forcing; a tropical cooling of 4^oC can only explain 8% of the glacial-interglacial pCO_2 change documented in ice cores.

1. Introduction

The main goal of this paper is to understand how changes in the surface boundary conditions affect the ocean circulation, the distribution of nutrients, and the atmospheric pCO_2. Inconsistency in the reconstruction of the glacial nutrient distribution in the Southern Ocean estimated from the carbon isotope ratio $\delta^{13}C$ and the ratio of cadmimum to calcium (Cd/Ca) of calcareous foraminifera shells obscured our view of the glacial ocean circulation [*Boyle*, 1992; *Broecker*, 1993; *Yu et al.*, 1996; *Francois et al.*, 1997]. Further, the 30% pCO_2 change of the last glacial-interglacial transition [*Barnola et al.*, 1987] is still unexplained [*Broecker and Henderson*, 1998; D. Archer et al., What causes the glacial-interglacial pCO_2 cycles?, submitted to *Reviews of Geophysics*, 1998; hereinafter referred to as Archer et al., submitted manuscript, 1998]. In this study we use the Hamburg Ocean Model of the Carbon Cycle (HAMOCC3) coupled on-line with the Hamburg large-scale geostrophic ocean general circulation model (LSG OGCM), which has been successfully applied for interannual and centennial climate studies [*Winguth et al.*, 1994; *Maier-Reimer et al.*, 1996]. The oceanic general circulation is forced by wind stress and exchange of heat and freshwater with the atmosphere. Attempts to reconstruct these boundary conditions for the Last Glacial Maximum (LGM) about 21,000 years ago lead to at least four critical questions [*Stocker*, 1998]: (1) What were the salinities in the area of LGM deepwater formation?, (2) Were the Nordic Seas ice-free during the glacial summer?, (3) What was the temperature of the tropical sea surface during the LGM?, and (4) What are the water mass characteristics of glacial Southern Ocean?

One category of ocean-modeling studies of the LGM consists of two-dimensional (2-D) and 3-D GCMs on the regional [*Schäfer-Neth*, 1994; *Seidov et al.*, 1996] and global scale [e.g., *Lautenschlager et al.*, 1992; *Fichefet et al.*, 1994; *Fieg*, 1996; *Winguth*, 1997; *Seidov and Haupt*, 1997; *Herterich et al.*, 1999] forced with specific restoring atmospheric GCM boundary conditions. Applications of regional models are problematic for past

Paper number 1999PA900002.
0883-8305/99/1999PA900002$12.00

climate states because they include not well known lateral boundary conditions. A second category of studies has used coupled models with reduced complexity of the glacial ocean-atmosphere system [*Ganopolski et al.*, 1998; *Weaver et al.*, 1998]. Fully coupled ocean-atmosphere GCMs have been integrated only over short periods (15 years)[*Bush and Philander*, 1998], by which the deep-ocean circulation is still far from equilibrium. Explicit flux adjustment, which is generally used to keep the fully coupled model simulations of the modern climate stable, could change significantly if different climate states were investigated.

Lautenschlager et al. [1992] suggested that strong model-data differences in the stable carbon isotopes ($\delta^{13}C$) could be reduced if instead of atmospheric general circulation models (AGCM), freshwater fluxes, restoring reconstructed salinities are used. The LGM salinities can be derived from analysis of stable oxygen isotopes in foraminifera shells [*Duplessy et al.*, 1991]. However, glacial salinity reconstruction suffers from errors in continental ice volume and temperature reconstructions as well as errors caused by the sea water $^{18}O/^{16}O$ ratio changes ($\delta^{18}O_w$) because of changes in freshwater input [*Mikolajewicz*, 1996]. Deviations of up to 0.5 in salinity from the modern linear salinity-$\delta^{18}O_w$ relation [*Labeyrie et al.*, 1992] are observed in the Southern Ocean because formation of sea ice influences salinity but has little impact on $\delta^{18}O_w$ [*Zahn and Mix*, 1991]. If the modern linear salinity-$\delta^{18}O_w$ relation is taken to reconstruct the glacial salinities, then large errors occur because of the imprecisely known extent of sea ice coverage and thickness.

Recent proxy data for sea surface temperature (SST) show discrepancies to the *Climate: Long Range Investigation, Mapping, and Prediction (CLIMAP) Project Members* [1981] reconstruction in polar and tropical regions [*Kellog*, 1980; *Duplessy et al.*, 1991; *de Vernal et al.*, 1993; *Hebbeln et al.*, 1994; *Weinelt et al.*, 1996; *Rosell-Melé and Koc*, 1997; A. de Vernal, personal communication, 1997]. These studies and results from the Global Environmental and Ecological Simulation of Interactive Systems (GENESIS) climate model [*Crowley and Baum*, 1997] support evidence for a warmer and less ice-covered glacial Atlantic than reconstructed by *CLIMAP Project Members* [1981]. Evidence from measurements of Sr/Ca in corals from Barbados [*Guilderson et al.*, 1994], noble gases in groundwater from Brazil [*Stute et al.*, 1995], alkenones [*Sikes and Keigwin*, 1994], and snow line depressions [*Rind and Peteet*, 1985] indicate also a reevaluation of LGM tropical SST with a 2°-4°C cooling below *CLIMAP Project Members* [1981]. Studies of the coupled atmosphere-ocean models support a global LGM cooling between 3.2° and 6.4°C [*Ganopolski et al.*, 1998; *Bush and Philander*, 1998; *Weaver et al.*, 1998].

Geological evidence from marine sediments indicates that glacial Southern Ocean surface winds were ~30-70% faster than at modern times [*Klinck and Smith*, 1993, and references therein]. *Toggweiler and Samuels* [1993] show with an OGCM a high sensitivity of the Atlantic overturning circulation to the strength of the West Wind Drift in the Southern Ocean.

In this study we will investigate how sensitive the deep-sea circulation, tracer distribution, and atmospheric pCO_2 respond to perturbations of forcing boundary conditions, i.e., to (1) high-latitude salinity, (2) tropical sea surface temperature, and (3) Southern Ocean winds in the range of their observational uncertainties. The results of these sensitivity experiments allow us to interpret the paleonutrient proxies from marine deep-sea sediment cores. Here we will focus on the paleonutrient tracers in the Atlantic, where most of the data have been sampled. The results of this study provide also a first guess for assimilation of paleonutrient proxies into an OGCM [*Winguth et al.*, 1998]. The data assimilation is computationally expensive, and solutions may converge to a secondary minimum. Emphasis must therefore be placed on a construction of a starting point for the assimilation, which is close enough to the geological data.

2. Model Description

2.1. Ocean General Circulation Model

The Hamburg large-scale geostrophic model (LSG) [*Maier-Reimer et al.*, 1993] is based on the conservation laws for heat, salt, and momentum (the latter in linearized form), the full equations of state, and the hydrostatic approximation. Gravity waves are suppressed by the implicit integration scheme, permitting a free sea surface elevation. The momentum equations are simplified by using the Boussinesq approximation and neglecting vertical friction. The circulation is divided into a barotropic component, denoting the vertically integrated circulation field, and baroclinic components, describing the vertical current shear. The motion outside the equator is essentially in geostrophic balance with frictional effects. Prognostic variables are sea ice, temperature, salinity, and geochemical tracers to which the velocities and surface elevation on the timescale of interest adjust almost immediately. The model runs on a global 72 x 72 E grid [*Arakawa and Lamb*, 1977] (approximate 3.5° x 3.5° horizontal resolution), uses 11 vertical layers with realistic bathymetry, and has a time step of 1 month in order to resolve the seasonal cycle. The temperature and salinity in the surface layer were computed by a Newtonian coupling to prescribed air temperatures and salinities with coupling coefficient of 40 W m^{-2} $^oC^{-1}$ and 1.5 x 10^{-5} m s^{-1}, yielding (for a 50 m thick top layer) a time constant for both prop-

erties of ~60 and 40 days. The ice model is a simple thermodynamic model including a wind-dependent ice advection [see *Mikolajewicz*, 1996].

2.2. Carbon Cycle Model

The model used here is the Hamburg Ocean Model of the Carbon Cycle (HAMOCC3) [*Maier-Reimer*, 1993] coupled on-line to the Hamburg LSG (hereafter HAMOCC3/LSG)[*Winguth et al.*, 1994; *Maier-Reimer et al.*, 1996]. Only a brief outline and modifications from *Maier-Reimer* [1993] are described in the following two subsections.

2.2.1. Nutrient cycle. The atmospheric pCO_2 and vertical gradients of carbon are linked with three pumping mechanisms [*Volk and Hoffert*, 1985]: the solubility pump with high solubilities at low temperatures and two biological pumps, the "soft tissue pump" caused by the formation of organic material and depletion of nutrients and carbon in the surface water and the $CaCO_3$ pump. Phosphate, well correlated in most parts of the ocean to nitrate, is chosen to be the limiting nutrient. Export production of phosphorus (NP), the part of primary production transported into deeper levels [*Eppley and Peterson*, 1979], is parameterized as by *Maier-Reimer* [1993] and depends on convective mixing Cc, light intensity I (as a function of latitude φ and time t), potential temperature ϑ (in degrees Celsius), and phosphate concentration (PO_4):

$$NP = r_0 \frac{50m}{Cc} I \frac{\vartheta + 2.}{\vartheta + 10.} \frac{PO_4{}^2}{P0 + PO_4} \quad (1)$$

Hence a temperature decrease of 1°C changes NP by 8% at 5°C and by 1% at 20°C. Cc is the depth of the convective column, $P0 = 0.02 \mu$mol L^{-1} denotes the half saturation concentration, and $r_0 = 0.25$ an adjustable constant to simulate a realistic surface phosphate. The model assumes a constant Redfield stoichiometry for particulate organic matter [*Takahashi et al.*, 1985].

$$P : N : C : \Delta O_2 = 1 : 16 : 127 : -172 \quad (2)$$

Much of the soft tissue sinks as fecal pellets or other large aggregates in a relatively short time compared to the circulation [*Honjo*, 1982]. Below the euphotic zone, which is represented by the top 50 m thick layer of the model, the downward flux of soft tissue is modeled according to *Berger et al.* [1987] proportionally to $(z/100 \text{ m})^{-0.8}$, where z denotes the depth in meters. A fraction of the downward flux of soft tissue (DMIN(K)) is assumed to remineralize in the Kth vertical layer. The original DMIN(K) of *Maier-Reimer* [1993] has been modified with an increase between 200 and 575 m by ~50% and a decrease by the corresponding amount in the two layers below to yield a better fit to the observed deep-sea phosphate concentrations in the eastern equatorial deep Atlantic. Overestimates of particulate organic material (POM or particulate organic carbon (POC)) are a consequence of an underestimation of the horizontal export of nutrients into subsurface layers of the eastern equatorial regions (i.e., top 500 m, referred to as nutrient trapping [*Najjar et al.*, 1992]). Remineralization of POC is limited to regions with sufficient oxygen. Unremineralized POC is preserved and advected by the circulation.

The total $\delta^{13}C$ ($\delta^{13}C_{tot}$) distribution can be described to first order as a combination of the carbon isotope fraction by the air-sea gas exchange ($\delta^{13}C_{as}$) and by biology ($\delta^{13}C_{bio}$)[*Broecker and Maier-Reimer*, 1992]. The $\delta^{13}C$ value for dissolved ΣCO_2 is well correlated to phosphate in most parts of the present-day deep ocean (below 1000 m)[*Kroopnick*, 1985; *Östlund et al.*, 1987], while surface water is affected by air-sea gas exchange and biology:

$$\delta^{13}C_{tot} = \delta^{13}C_{as} + \delta^{13}C_{bio} \quad (3a)$$

where

$$\delta^{13}C_{bio} = \begin{cases} 2.7 - 1.1\, PO_4 & \text{for present day} \\ 2.5 - 1.0\, PO_4 & \text{for the LGM} \end{cases} \quad (3b)$$

Equation (3a) allows us to compute the effect of the air-sea gas exchange $\delta^{13}C_{as}$ from PO_4 and $\delta^{13}C_{tot}$ (treated similar to *Maier-Reimer* [1993]). The estimation of $\delta^{13}C_{bio}$ is based on a mean concentration of 2200 μmol kg^{-1} for ΣCO_2 and 2.2 μmol kg^{-1} for PO_4. In formula (3b) we assume a constant fractionation for organic matter of -20‰ for modern times and -18‰ for the LGM [*Rau et al.*, 1991]. *Rau et al.* [1991] indicate that the fractionation effect in organic matter depends on the temperature and local concentration of dissolved CO_2. Measurements of CO_2 in surface waters and $\delta^{13}C$ in organic material sustain a relationship between these two properties [*Altabet*, 1996], but this is not supported by the sensitivity studies of *Maier-Reimer* [1993].

2.2.2. CO_2 gas exchange for stable carbon isotopes. The model includes a zonally averaged diffusive atmosphere module, which has the same horizontal resolution as the ocean model and an interhemispherical mixing of ~1 year. The net flux of carbon isotopes C^{12} and C^{13} (F^{12} and F^{13}) is proportional to the difference between the atmospheric and ocean pCO_2 [*Siegenthaler and Münnich*, 1981]:

$$F^{12} = F_{as} - F_{sa} = \lambda (P_a - P_s) \quad (4)$$

$$F^{13} = \alpha_{as} F_{as} R_a^{13} - \alpha_{sa} F_{sa} R_s^{13} \quad (5)$$

where P_a denotes the partial pressure of the CO_2 gas and R_a the $^{13}C/^{12}C$ ratio in the atmosphere, P_s denotes the partial pressure of the sea surface, and R_s denotes the $^{13}C/^{12}C$ ratio in oceanic carbon. In this

study we choose a spatially and seasonally constant bulk coefficient λ as a first-order approximation according to *Lynch-Stieglitz et al.* [1995]. The bulk coefficient has a value of 0.06 mol m^{-2} ppm^{-1} yr^{-1} to match the *Broecker et al.* [1986] estimate from the uptake of bomb radiocarbon. The concentration $[CO_2]$ determines the CO_2 partial pressure in the ocean by $P_s = [CO_2]/\beta$ (β denotes the solubility of CO_2 in seawater; for details, see *Maier-Reimer and Hasselmann* [1987]). The P_s rises by ~14 ppm with a 1.6°C global glacial to interglacial shift according to *CLIMAP Project Members* [1981] and sinks by 1.4 ppm if salinity is decreased from 35.7 to 34.7 [*Weiss*, 1974]. The isotopic fractionation on the surface reflects a lower tendency of the heavier isotope to evaporate [*Vogel et al.*, 1970; *Mook et al.*, 1974; *Maier-Reimer*, 1993]:

$$\alpha_{as} = [-0.373/(\vartheta + 273.15) + 1.00019]\,\alpha_k \quad (6)$$

$$\alpha_{sa} = [1.02389 - 9.483/(\vartheta + 273.15)]\,\alpha_k \quad (7)$$

where ϑ is the SST in °C and $\alpha_k = 0.9995$ is the kinetic fractionation factor [*Siegenthaler and Münnich*, 1981]. A cooling of 1°C would thus enrich in equilibrium the ocean surface relative to the atmosphere by ~0.1‰.

3. Data

The $\delta^{13}C$ data are taken from analysis of benthic foraminiferal shells from studies of *Sarnthein et al.* [1994] and *Michel* [1995] for the modern (0-4 ka) and the LGM (21.5-23.5 ka) time slice. The analytical reproducibility of $\delta^{13}C$ is up to ±0.04‰ for $\delta^{13}C$ (Kiel laboratory) [*Sarnthein et al.*, 1994]. However, deviations between $\delta^{13}C$ measurements of the foraminiferal shells and dissolved inorganic carbon (DIC) in deep water are much larger, of the order of ±0.2‰ as shown by *Sarnthein et al.* [1994, Figure 6 (b)] or by *McCorkle and Keigwin* [1994]. Here we assume the same observational error of ±0.2‰ as in the study of *LeGrand and Wunsch* [1995]. The $\delta^{13}C$ value in *Fontbotia wuellerstorfi* differs up to -0.5‰ from the ratio in the surrounding bottom water dependent upon seasonal flux rates of organic carbon and $\delta^{13}C$ of pore water DIC (Mackensen effect) [*Mackensen et al.*, 1993; *Bickert and Wefer*, 1996; *Mackensen*, 1997]. The $\delta^{13}C$ value in the deep Atlantic can be approximated by the effect of the biological pump $\delta^{13}C_{tot} \approx \delta^{13}C_{bio*} = \delta^{13}C_{bio} + c$, where c is a constant chosen to be -0.2‰ for modern times. The glacial-interglacial change of -0.4‰ in the deep Pacific cores implies a ~600 Gigatons carbon (GtC, 1 GtC = 10^{12} kg C) loss during glacial times from land biosphere (see *Crowley* [1995] for a review). Glacial-interglacial changes in the land biosphere were recently estimated to be 850 ±300 GtC [*Crowley*, 1995, Table 2] and carbon and $\delta^{13}C$ deficits of the land biosphere were estimated to be 250 ±300 GtC and 0.2 ±0.2 ‰, respectively. The observed -0.4‰ shift can be possibly explained alone by a higher pH of seawater during glacial times [*Sanyal et al.*, 1995] if a pH dependence on the $^{13}C/^{12}C$ of calcareous foraminiferal shells is considered [*Spero et al.*, 1997].

Cd/Ca in the water column follows in first-order phosphorus (P) in the ocean with the "global" Cd-P relationship (Cd=0.208P for P<1.34 and Cd=0.279+ 0.398(P-1.34) for P>1.34) [*Boyle*, 1988]. Here we used the method from *Boyle* [1992] to transform the Cd/Ca data from the foraminifera shells into phosphate concentrations of the water column which can be directly compared with the simulated phosphate values. Cd distribution coefficients between Cd (foram) and Cd (water) are taken from a depth dependence relationship (1.3 for z <1150 m, 1.3+(z-1150)(1.6/1850) for 1150 m <z<3000 m, and 2.9 for z >3000 m) [*Boyle*, 1992]. Here we use the Cd/Ca data set by *Boyle* [1992].

4. Experiments

Long-term variations of the ocean circulation are influenced by changes of sea surface boundary conditions (temperature, salinity, and momentum fluxes) as well as changes in sea level and bottom topography. Ten sensitivity experiments with different interglacial and glacial boundary conditions were carried out (Table 1).

For all glacial-type experiments, sea level was reduced by 120 m [*Fairbanks*, 1989], which increases the average marine tracer concentration by ~3%, and the Bering Strait was closed. All experiments were integrated (of order 10,000 years and more) with the forcing fields until a steady state of the circulation and an equilibrium of the stable carbon isotopes were achieved. The glacial experiments with HAMOCC3/LSG were spun up from the reference experiment Interglacial First Guess (IFG).

4.1. Reference Experiment IFG With Modern Boundary Conditions

In the reference experiment we used monthly mean Comprehensive Ocean-Atmosphere Data Set (COADS) air temperatures [*Woodruff et al.*, 1987], annual mean climatological sea surface salinities from *Levitus* [1982], and monthly mean wind stress from the control run of the European Centre/Hamburg atmospheric general circulation model (ECHAM3/T42) [*Lorenz et al.*, 1996] as modern boundary conditions. The circulation state and tracer distribution with these boundary conditions are comparable with those from the reference run (ATOS1) produced by *Maier-Reimer et al.* [1993] (Table 2 and Figures 1-3).

The carbon cycle model was spun up from the reference experiments of *Maier-Reimer et al.* [1996]. The global mean concentrations (PO_4 = 2.1 μmol L^{-1}, DIC = 2239 μmol L^{-1}, and total alkalinity (TAlk) =

Table 1. Overview of Sensitivity Experiments

Experiment[a]	Surface Boundary Condition		
	Temperature[b]	Salinity[c]	Wind Stress[d]
IFG	ECHAM3/T42(Modern)	Levitus	ECHAM3/T42 (Modern)
GFGNC	ECHAM3/T42(LGMC)	Levitus+Duplessy	ECHAM3/T42 (LGMC)
GFG	ECHAM3/T42(LGMC)	Levitus+Duplessy+ΔS	ECHAM3/T42 (LGMC)
GFGP1	ECHAM3/T42(LGMC)	Levitus+Duplessy+ΔS North Atlantic (>50°N): +1	ECHAM3/T42 (LGMC)
GFGM1	ECHAM3/T42(LGMC)	Levitus+Duplessy+ΔS North Atlantic (>50°N): -1	ECHAM3/T42 (LGMC)
GFGWSN	ECHAM3/T42(LGMW)	Levitus+Duplessy+ΔS North Atlantic: Schäfer-Neth	ECHAM3/T42 (LGMW)
GFGTC2	ECHAM3/T42(LGMC) Tropics: -2°C	Levitus+Duplessy+ΔS	ECHAM3/T42 (LGMC)
GFGTC4	ECHAM3/T42(LGMC) Tropics: -4°C	Levitus+Duplessy+ΔS	ECHAM3/T42 (LGMC)
GFGHW	ECHAM3/T42(Modern)	Levitus+Duplessy+ΔS	ECHAM3/T42 (LGMC)
GFGSW	ECHAM3/T42(LGMC)	Levitus+Duplessy	ECHAM3/T42 (LGMC) ACC: $1.5\tau_x$

[a]IFG, Interglacial First Guess (reference run) with present-day boundary conditions; GFGNC and GFG, Glacial First Guess with Last Glacial Maximum (LGM) boundary conditions; GFGP1 and GFGM1, experiments with additional anomalies of ±1 in salinity in the North Atlantic; GFGWSN, an experiment with warmer and more saline boundary conditions in the Nordic Seas; GFGTC2 and GFGTC4, experiments with cooling of tropical 2 m air temperature by 2°C and 4°C; GFGHW, an experiment with modern wind stress but, otherwise, glacial boundary conditions; and GFGSW, an experiment in which glacial wind stress in the Southern Ocean was intensified in the zonal component by a factor of 1.5 (see Figure 9).

[b]ECHAM3/T42, European Centre/Hamburg atmospheric general circulation model; LGMC uses sea surface temperatures (SSTs) from *CLIMAP Project Members* [1981]; and LGMW uses SSTs from *Weinelt et al.* [1996] in the Nordic sea but otherwise uses SSTs from *CLIMAP Project Members* [1981].

[c] Levitus, *Levitus* [1982]; Duplessy, *Duplessy et al.* [1991,1996]; ΔS denotes a correction of -0.5 in salinity in the North Atlantic and +0.5 in salinity in the South Atlantic; and Schäfer-Neth, *Schäfer-Neth* [1994].

[d]ACC, Antartic Circumpolar Current.

Table 2. Results of Sensitivity Experiments

	Experiment						
	IFG	GFG	GFGWSN	GFGP1	GFGM1	GFGHW	GFGSW
Heatflux, PW[a]							
North Atlantic	0.89	0.72	0.58	1.08	0.46	0.54	0.78
relative convective E_{pot}							
ACC/global[b], %	69	86	89	70	92	87	87
Transports, Sv							
Atlantic	-17.5	-7.9	-7.8	-20.7	-1.4	-7.3	-10.7
Pacific	17.3	25.3	22.6	26.5	24.8	19.7	25.6
Indian	12.9	10.2	11.1	12.1	8.8	10.2	10.6
Drake Passage	112.3	125.8	126.5	114.8	131.5	121.5	137.4
Potential temperature, °C							
> 1500m	1.96	0.74	0.87	0.82	0.80	0.79	0.86
global	3.78	2.26	2.31	2.22	2.38	2.40	2.32
Salinity							
> 1500m	34.78	36.15	36.13	36.26	36.13	36.21	36.12
global	34.80	36.13	36.10	36.22	36.12	36.19	36.10
Export Production, GtC $month^{-1}$	0.97	1.05	1.04	1.06	1.02	0.95	1.10
Atmospheric pCO_2, ppm	279.3	280.0	279.9	280.3	279.5	278.7	287.4

Northward respectively eastward transports have positive values.

[a]Integrated heatflux in PW (10^{15} W) at 30°N.

[b]Relation of relative potential energy loss by convection between Southern Ocean and the global ocean.

[c]Zonally integrated transports at 30°S between 1500 and 3500 m depth.

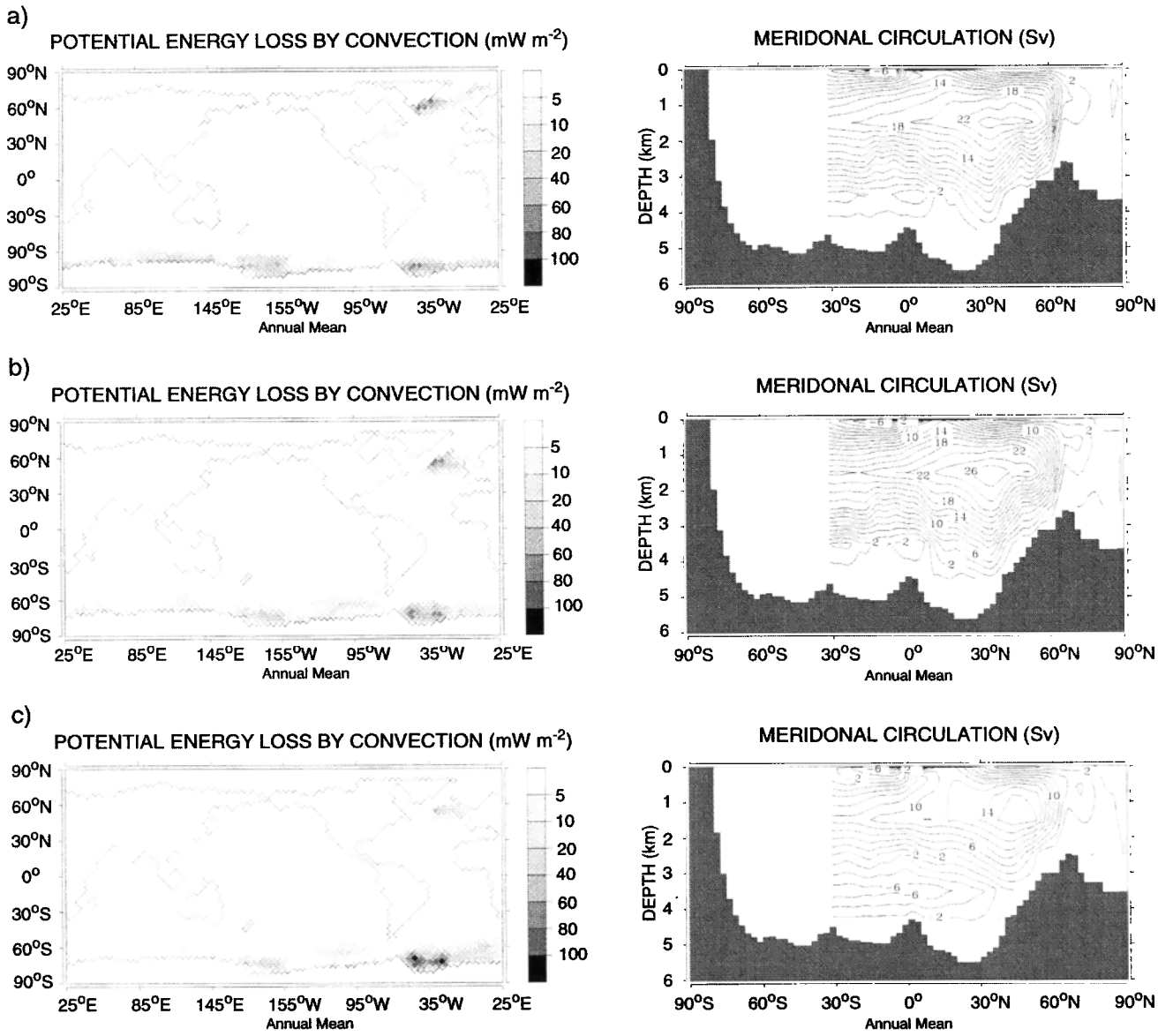

Figure 1. Ocean general circulation model (OGCM) response to modern and Last Glacial Maximum boundary conditions: experiment (a) Interglacial First Guess (IFG), (b) Glacial First Guess With No Salinity Corrections (GFGNC), and (c) Glacial First Guess (GFG). (left) Potential energy loss due to convection (contour interval: mW m^{-1}). (right) Zonally averaged Atlantic meridional circulation (contour interval: 1 Sv = 10^6 m^3 s^{-1}).

2383 μeq L^{-1}) are adjusted to be in equilibrium with a preanthropogenic atmospheric pCO_2 of ~280 ppm. Atmospheric $\delta^{13}C$ is adapted to be -6.5‰ according to *Friedli et al.* [1986]. Simulated phosphate in the Atlantic reflects generally the different water properties (Figure 4a). North Atlantic Deep Water (NADW) has a low nutrient concentration, while high phosphate concentrations are accompanied with deeper Antarctic Bottom Water (AABW or South Component Water (SCW)). The eastern boundaries and equatorial areas of the oceans are characterized by high biological activity due to Ekman transport-induced upwelling (Figure 3c) of nutrients from deeper levels and their advection in westward direction. Simulated phosphate in the tropical intermediate layers is higher than observations of *Conkright et al.* [1994] as an artifact of nutrient trapping.

The $\delta^{13}C_{tot}$ inversely follows phosphate in layers below 1000 m. For comparison, observations after a data set of *Kroopnick* [1985] are displayed in Figure 5. Most of the misfits between the modeled $\delta^{13}C_{bio*}$ distribution and the data from foraminifera shells (*Fontbotia wuellerstorfi*) (Table 3) have deviations in the size of the assumed 0.2‰ error range of the data themselves. Ar-

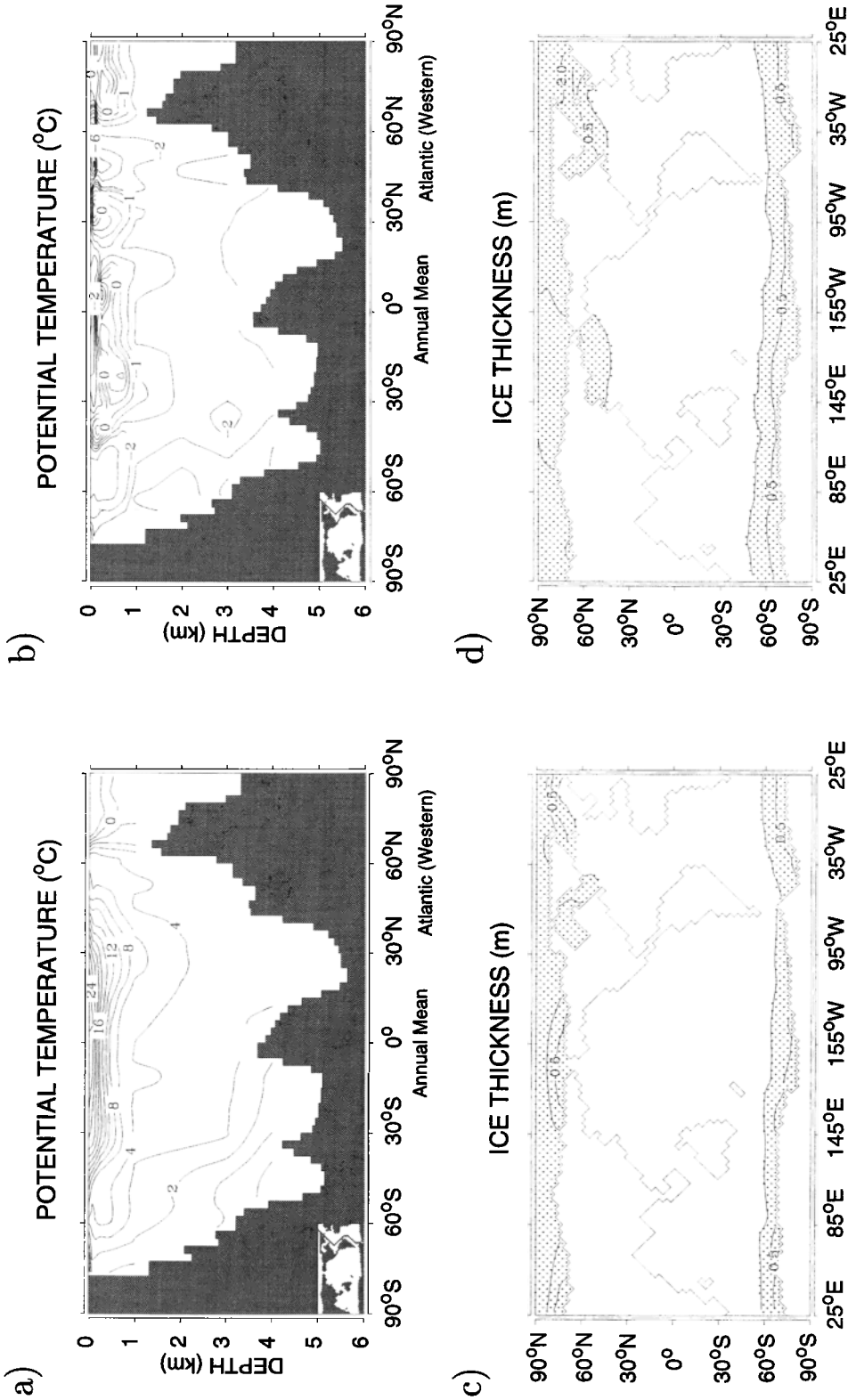

Figure 2. OGCM response to modern and LGM boundary conditions. Potential temperature in degrees Celcius in the western Atlantic. ((a) experiment IFG and (b) difference experiment GFG minus IFG), and ice thickness ((c) experiment IFG and (d) GFG; contour interval: 0.5 m).

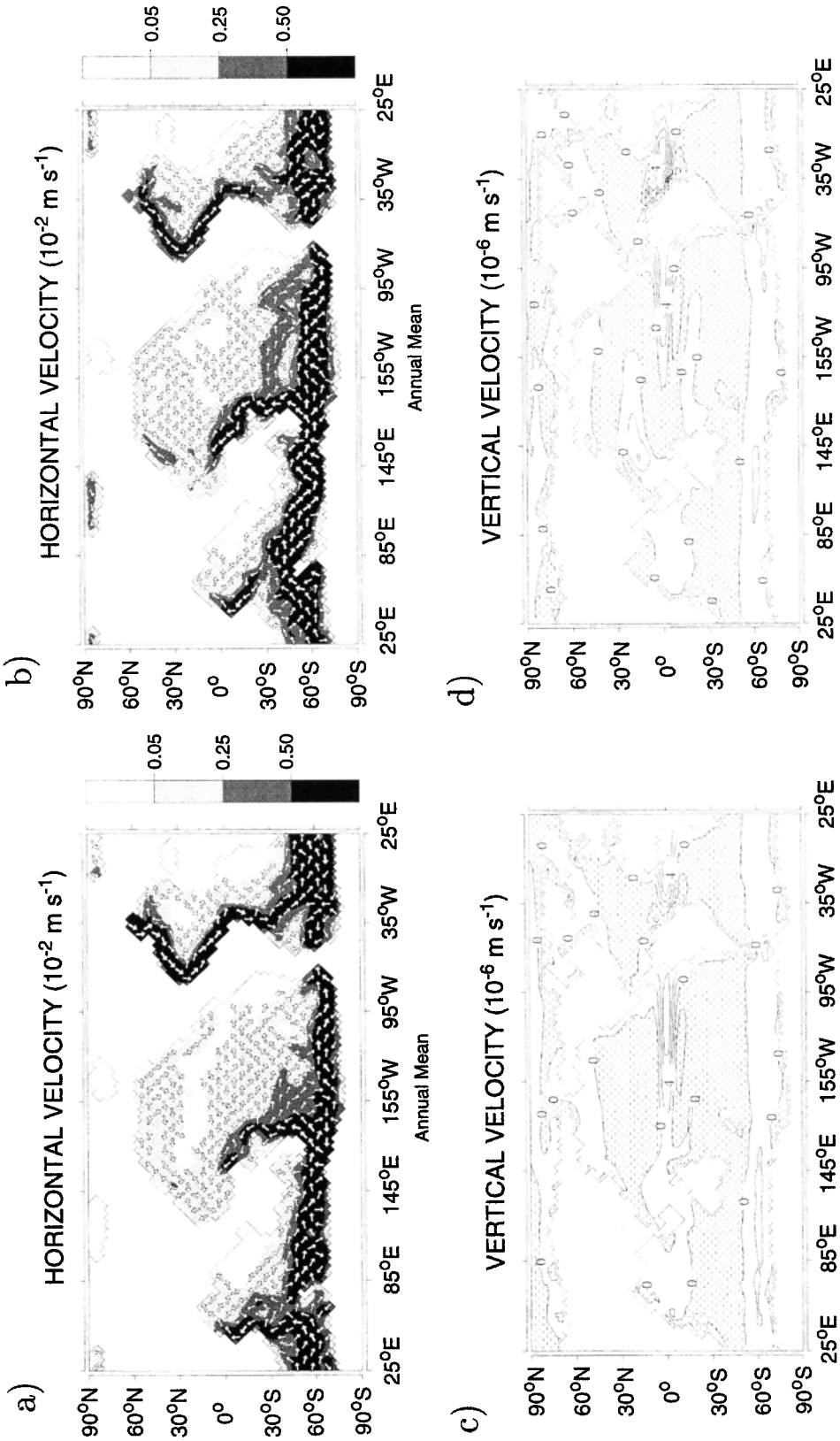

Figure 3. OGCM response to modern and LGM boundary conditions ((left) experiment IFG and (right) GFG). (a) and (b) Horizontal velocities in 3000 m and (c) and (d) vertical velocity between surface layer and second model layer (contour interval: 2×10^{-6} m s^{-1}).

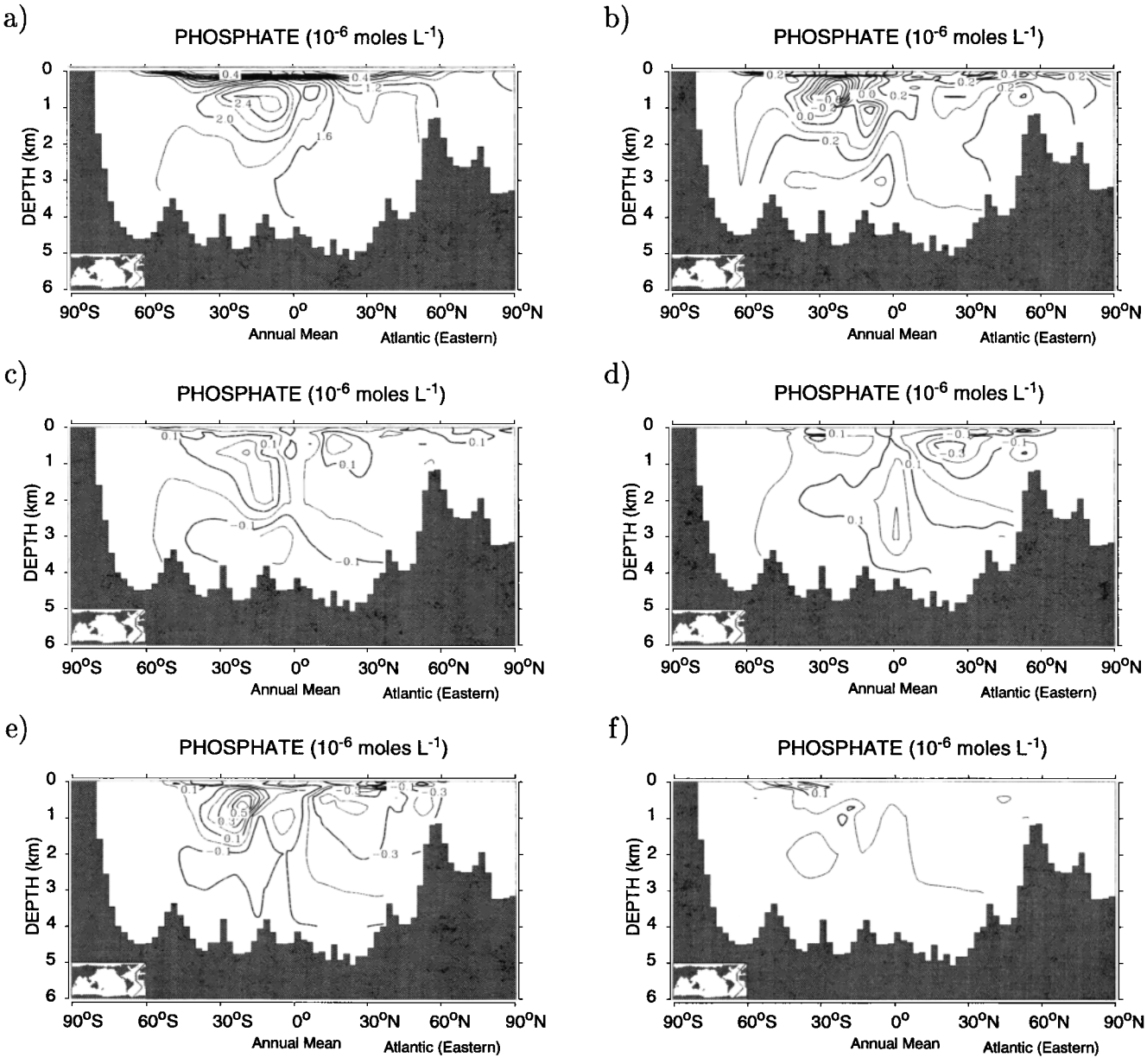

Figure 4. Meridional phosphate section across the eastern Atlantic simulated by an OGCM for experiments (a) IFG, and differences (b) GFG-IFG, (c) GFG with an additional anomaly of +1 in salinity in the North Atlantic (GFGP1)-GFG, (d) GFG with an additional anomaly of -1 in salinity in the North Atlantic (GFGM1)-GFG, (e) GFG with modern wind stress (GFGHW)-GFG, and (f) GFG with wind intensified by 50% in the Southern Ocean (GFGSW)-GFG. Contour interval 0.1 μmol l^{-1}.

eas of concordance between data and modeled counterparts are assigned to the western, northern, and southern Atlantic, while deviations occur in the tropical regions. The differences from Cd/Ca data in Table 3 indicate that the deviations in this region are partly related to the nutrient trapping. The effect of $\delta^{13}C$ gas exchange ($\delta^{13}C_{as}$) for the modern eastern Atlantic is displayed in Figure 6a. At the ocean surface, deviations from the biological effect are mainly due to the temperature dependence of the gas exchange formulation (Figure 6a). Cold water like the Southern Ocean tends to have more kinetic fractionation and thus higher $\delta^{13}C$ values than warm waters of the subtopical gyres with mostly positive values (Figure 2a). The weak effect of the gas exchange in the deep sea supports previous findings of *Broecker and Maier-Reimer* [1992] and *Lynch-Stieglitz et al.* [1995].

4.2. The Glacial Flow Field

The use of atmospheric forcing data (prescribed monthly mean air temperatures and wind stress derived from the LGM experiment with the atmospheric general

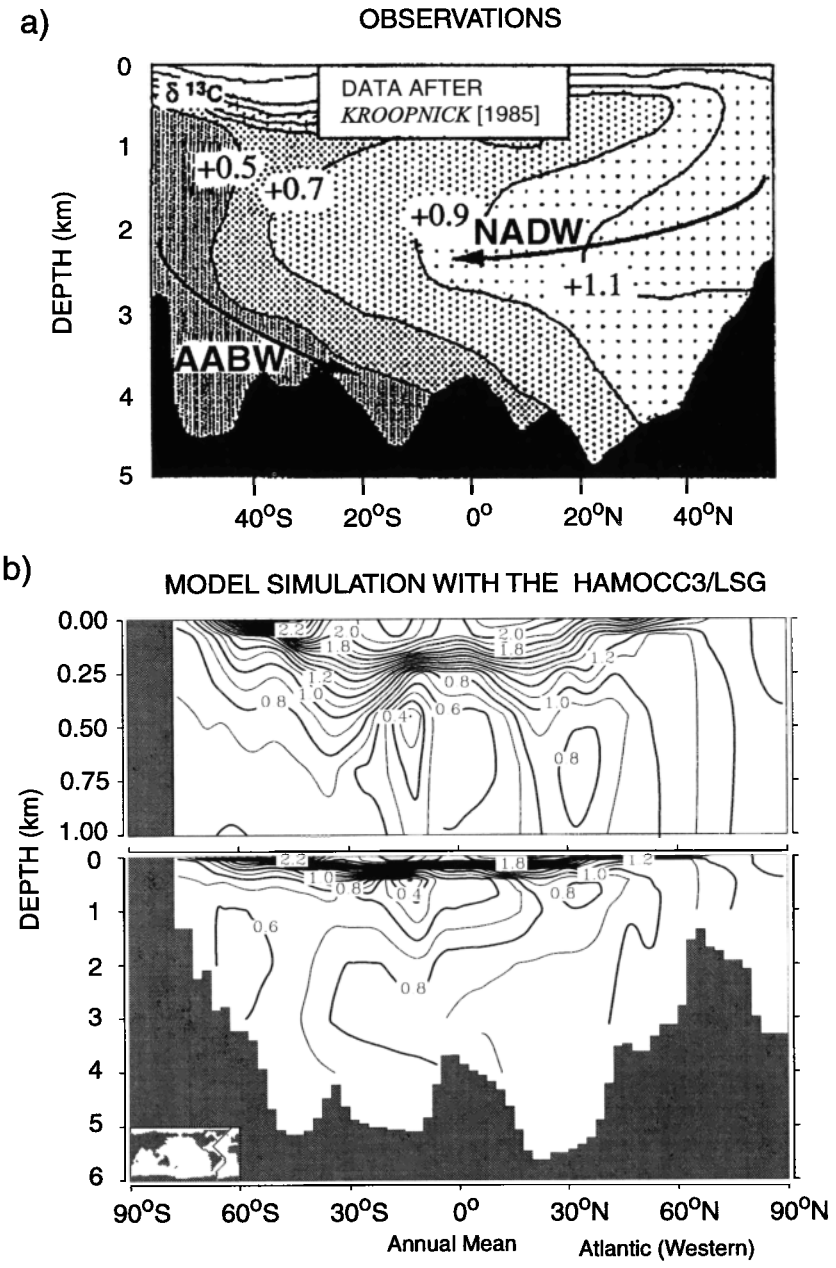

Figure 5. Distribution of $\delta^{13}C_{tot}$ in the western Atlantic (modern interglacial period): (a) Observations adapted from *Kroopnick* [1985] and (b) OGCM response to modern boundary conditions (experiment IFG).

circulation model ECHAM3/T42 [*Lorenz et al.*, 1996]), although they incorporate shortcomings of the formulation of the AGCM and its boundary conditions, is a first step toward a coupled atmospheric-oceanic climate system. However, the use of LGM freshwater fluxes as a boundary condition has led to significant discrepancies between the simulated and reconstructed distribution of the paleonutrients and radiocarbon [*Lautenschlager et al.*, 1992]. Hence glacial salinity fields were estimated by modern climatology [*Levitus*, 1982] and anomalies gained from salinity reconstructions of *Duplessy et al.* [1991, 1996] (Figure 7). The reconstructions from $\delta^{18}O$ in foraminiferal shells are interpolated to the model grid by advection with the "North Component Water (NCW)-reduced" mode of *Mikolajewicz et al.* [1993] including a global +1 increase in salinity. The experiment with these boundary conditions is named Glacial First Guess With No Salinity Corrections (GFGNC).

The steady state solution with these glacial boundary conditions generates strong convection (Figure 1b) along the ice margin in the central North Atlantic south of Iceland, driven by cold SSTs and relatively

Table 3. Root Mean Square Error Between Simulated Values by an Ocean General Circulation Model (OGCM) and Paleonutrient Data in the Atlantic Ocean

	$\delta^{13}C_{bio*}$								Cd/Ca		
	IFG	GFGNC	GFG	GFGWSN	GFGP1	GFGM1	GFGHW	GFGSW	IFG	GFGNC	GFG
60°- 45°N	0.22	0.36	0.37	0.37	0.41	0.35	0.32	0.39	0.37	0.33	0.31
45°- 30°N	0.19	0.30	0.33	0.33	0.42	0.28	0.32	0.35	0.35	0.24	0.25
30°- 15°N	0.15	0.36	0.33	0.34	0.38	0.25	0.40	0.34	0.28	0.38	0.36
15°- 0°N	0.30	0.50	0.47	0.47	0.48	0.52	0.51	0.47	0.29	0.57	0.44
0°- 15°S	0.58	0.64	0.78	0.77	0.80	0.86	0.79	0.78	0.43	0.34	0.41
15°- 30°S	0.35	0.36	0.24	0.25	0.33	0.25	0.30	0.24	0.37	0.26	0.29
30°- 45°S	0.17	0.41	0.39	0.39	0.43	0.38	0.44	0.39	0.27	0.25	0.18
45°- 60°S	0.04	0.80	0.66	0.66	0.72	0.62	0.76	0.68	...	...	...
Atlantic	0.29	0.44	0.43	0.43	0.47	0.45	0.46	0.44	0.32	0.38	0.34

The $\delta^{13}C$ data are after *Sarnthein et al.* [1994] and *Michel et al.* [1995]; the Cd/Ca ratios are after *Boyle* [1992]. Only grid points in the nearest vicinity to the position of the marine sediment cores are considered.

high salinities, and a southward outflow of the NCW even stronger than the present-day simulation (IFG). These model results do not support the view of the glacial circulation from paleonutrient measurements in foraminiferal shells as proposed by, for example, *Curry and Lohmann* [1983], *Boyle and Keigwin* [1987], *Duplessy et al.* [1988], and *Sarnthein et al.* [1994].

In a second experiment, the Glacial First Guess (GFG), we modified sea surface salinities in the high latitudes within the observational uncertainty to reduce the model-data misfit of paleonutrients (Table 3). A typical ±1°C deviation in the temperature reconstruction introduces a ±0.25‰ difference in $\delta^{18}O_w$ and a ±0.5 difference in the salinity reconstruction [*Labeyrie et al.*, 1992]. Applying the modern linear salinity-$\delta^{18}O_w$ relation for glacial times can cause even larger errors [*Mikolajewicz*, 1996]. The prescribed buoyancy fluxes in the Atlantic were lowered by a negative anomaly of -0.5 in salinity north of 50°N and increased by a positive anomaly of +0.5 in salinity south of 50°S (with a linear transition between 40° and 50°). The extent of sea ice (Figure 2d) can be interpreted as a consequence of the use of 2 m air temperatures derived from *CLIMAP Project Members* [1981]. Main areas of the North Atlantic Deep Water formation (Figure 1c) are located south of Iceland and south of the sea ice margin around 40°N, in agreement with interpretations of oxygen and carbon isotope measurements from *Labeyrie et al.* [1992] and *Sarnthein et al.* [1994], and produce 2°-3°C cooler water below modern NADW (Figure 2b). The change of the buoyancy fluxes in the polar regions (reduced convective overturning in the North Atlantic and slightly intensified Southern Ocean Deep Water source; Figure 1c) causes a reduced deep western boundary current (Figure 3b) and a 50% reduced outflow (below 1500 m) at 30°S into the Southern Ocean. Similar reduction rates have been simulated by the use of other GCMs [*Fichefet et al.*, 1994; *Seidov and Haupt*, 1997; *Herterich et al.*, 1999]. The increased ventilation of the deep Pacific is at odds with radiocarbon data, indicating a less ventilated central deep Pacific [*Shackleton et al.*, 1988; *Broecker et al.*, 1988]. A source of glacial North Pacific Deep Water [*Keigwin et al.*, 1992], missing in our simulation, would significantly dampen the inflow into the deep Pacific [*Lautenschlager et al.*, 1992]. The main branch of the Antarctic Circumpolar Current (ACC) shifted northward and increased in strength from 115 Sv to 125 Sv because of a 10% increase in wind stress predicted by the AGCM and an intensified density gradient on the ice margin (Figure 8 and Table 2). The wind stress predicted by the AGCM is ~20-60% lower than estimates from marine sediment records [*Klinck and Smith*, 1993].

The meridional heat transport, depending strongly on the forcing CLIMAP temperatures, is characterized by a reduced northward transport in the northern Atlantic (Figure 9). In contrast to the interglacial experiment, the model predicts negative values and a southward transport for the South Atlantic. *Webb et al.* [1997] found, with an AGCM coupled to a slab ocean, enhanced tropical cooling during glacial times if modern heat transport is used, but otherwise, glacial boundary conditions are applied.

High phosphate concentrations in the deep central Atlantic (Figure 4b) are a combined result of an intensification of the Southern Ocean source and an intensification of the export production linked to the 20% increase in Ekman-induced upwelling (Figure 3d). The latter is in agreement with geological reconstructions [e.g., *CLIMAP Project Members*, 1981; *Sarnthein et al.*, 1988; *Yu et al.*, 1996]. In the Southern Ocean, small changes of phosphate concentration resemble the Cd/Ca measurements and cannot explain the observed shifts in $\delta^{13}C$ (Table 3). Differences in $\delta^{13}C_{as}$ between

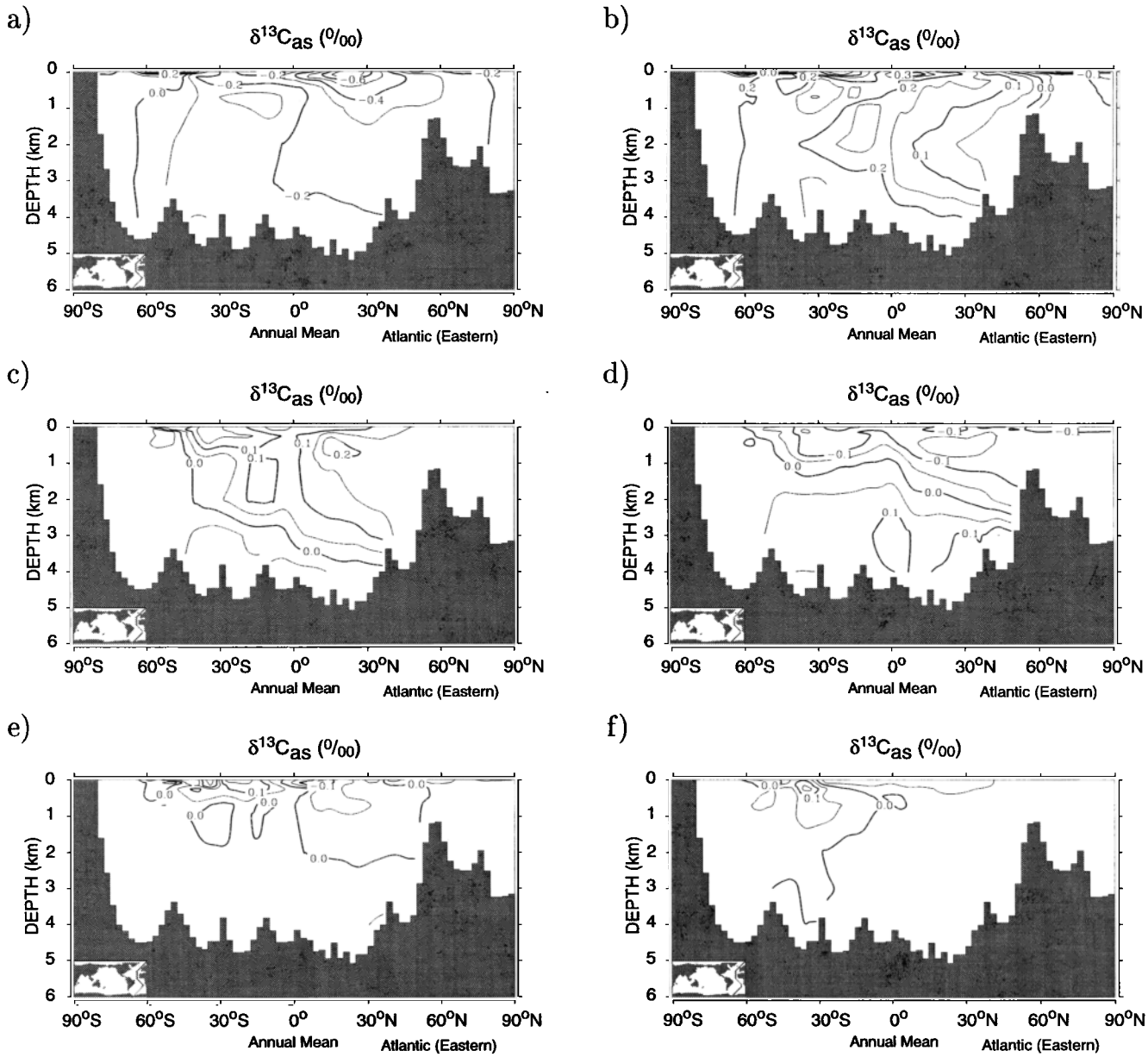

Figure 6. Meridional section of the effect of gas exchange $\delta^{13}C_{as}$ across the eastern Atlantic simulated by an OGCM for (a) IFG (contour interval 0.1 ‰) and differences (b) GFG-IFG, (c) GFGP1-GFG, (d) GFGM1-GFG, (e) GFGHW-GFG, and (f) GFGSW-GFG (contour interval 0.05 ‰).

GFG and IFG are positive in this area because of glacial cooling and cause an even stronger discrepancy (Figure 6b). The simulated cool glacial NCW has a higher $\delta^{13}C_{as}$, as supported by analysis of stable carbon isotope and Cd/Ca data [*Lynch-Stieglitz and Fairbanks*, 1994]. *Lynch-Stieglitz and Fairbanks* [1994] estimates of glacial to interglacial change in the gas exchange of 0.6-1.0‰ at 1-2 km depth seems to be in conflict, however, with very light $\delta^{13}C$ in the glacial Nordic Seas [*Sarnthein et al.*, 1995].

The atmospheric pCO_2 is only weakly affected by the glacial-interglacial changes of the boundary conditions and circulation (ΔpCO_2 ~8%; Table 2). The changes are mainly attributed to changes of the upwelling of nutrient-rich water in the tropics. The relatively small changes in the nutrient cycle do not cause significant changes of carbon transfer from the surface into the deep sea. The effect of changes in the CO_2 solubility by colder glacial water is mainly compensated by the reorganization of the tracers due to an increase in con-

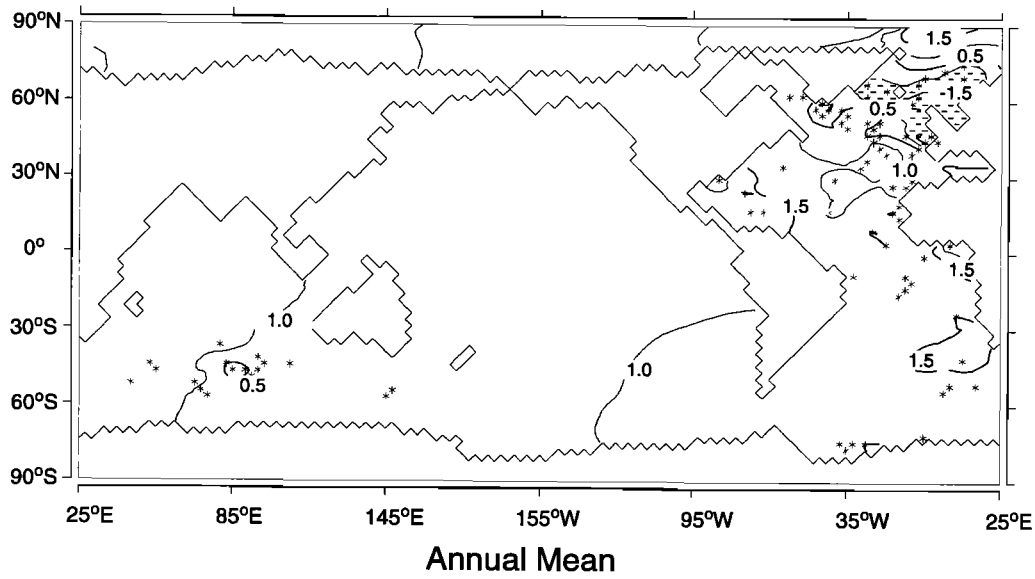

Figure 7. Reconstruction of glacial-interglacial salinity anomaly at the sea surface from analysis of stable oxygen isotopes in foraminifera shells [*Duplessy et al.*, 1991,1996]. A global +1 increase in salinity due to the storage of water in the great Laurentide and Fennoscandian Ice Sheets is included. The sparsely distributed reconstructed salinity values were interpolated to the model grid by advection with the NCW-reduced mode of *Mikolajewicz et al.* [1993]. Stars denote geographical position of data. The contour interval is 0.5.

centration caused by the lower sea level assumed for glacial times. However, uncertainties still exist because of the uncertainties of the model formulation and poorly known boundary conditions, especially in the Southern Ocean.

4.3. Sensitivity to LGM Salinity and Temperature Boundary Conditions in the North Atlantic

Changes in high-latitude buoyancy fluxes are essentially an extrapolation of the theoretical calculations of *Stommel and Arons* [1960]. In GFGP1 an anomaly of +1 in salinity north of 50°N (with a linear transition to 40°N) causes an intensification of the deepwater formation in the North Atlantic and an increase of the southward outflow of NCW, which is about twice as strong as in GFG (Table 2 and Figures 10a and 10b). The strong southward deep outflow is compensated by an increased northward flow and heat transport on the surface. In contrast, in GFGM1 the salinity anomaly of -1 causes almost a breakdown of the Atlantic overturning circulation and western boundary currents. Transports through the Drake Passage are modeled to be 115 Sv for GFGP1 (~10% lower than GFG) and 132 Sv for GFGM1 (~10% higher than GFG). These changes reflect the inverse behavior of the strength of the ACC at the Drake Passage to the relative strength (in terms of potential energy) between the North Atlantic source and the source in the Southern Ocean.

An additional experiment, GFG With Warmer and More Saline Boundary Conditions in the Nordic Seas (GFGWSN), has been carried out to study the effect of a less icy Greenland Sea during the glacial summer. We have chosen 2 m air temperatures and wind stress from an AGCM experiment (G. Hoffmann, personal communication, 1996) using SST from *Weinelt et al.* [1996]. Surface salinities in the Nordic Seas for this experiment are calculated from foraminiferal $\delta^{18}O$ measurements and transfer function SST estimates. They are spatially interpolated with the Modular Ocean Model (MOM) [*Schäfer-Neth*, 1994]. In regions other than the northern North Atlantic the boundary conditions are the same as for GFG. Gulf Stream and northward heat transport in GFGWSN are slightly weaker than in GFG, and the thermohaline circulation is reduced, mainly because of the comparably less dense North Atlantic water masses in GFG.

Advection of cold air masses from the Greenland ice sheet has caused too strong a cooling of the simulated SST because of a lack of spatial resolution of the atmospheric and ocean GCMs. Hence the strength of the northern source is similar to GFG and might be overestimated. Differences between GFGWSN and GFG are small and are thus not further discussed.

The export production increases with relative salinity (Figure 11a). A stronger Atlantic overturning circulation reduces the stratification of nutrients and hence increases the export of carbon. North to south contrast of

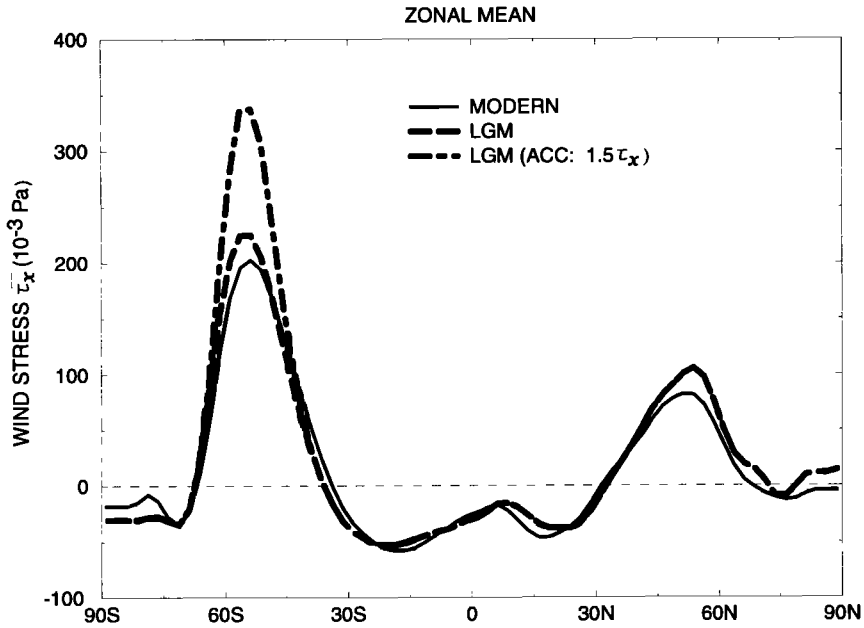

Figure 8. Average zonal component of wind stress in response to present-day boundary conditions (solid, thin line), LGM boundary conditions (dashed, thick line), and LGM boundary conditions including an increase by a factor of 1.5 in the region between 67.5°S and 40°S (dot-dashed, thick line). The zonal components of wind stress were computed from experiments with the European Centre/Hamburg Atmospheric General Circulation Model (ECHAM3/T42).

phosphate concentration (Figures 4c and 4d) and $\delta^{13}C_{as}$ (Figures 6c and 6d) in the deep sea increases with a decrease of the overturning circulation and reflects the influence of the water properties NCW versus SCW. Changes in these properties are small, and hence the pCO_2 does not change significantly. Figure 11b reflects also, in part, changes in solubility of NCW (higher salinity decreases the solubility).

4.4. Sensitivity to Tropical Sea Surface Temperatures

Recent Sr/Ca measurements in glacial age corals in the vicinity of Barbados indicate that during the LGM, tropical SSTs were up to 4°C lower [*Guilderson et al.*, 1994], as estimated from *CLIMAP Project Members* [1981]. To investigate the relation between lower tropical SST and the atmospheric pCO_2, prescribed 2 m air temperatures have been lowered in experiment GFG Tropical Cooling by 2°C (GFGTC2) and by 4°C (GFGTC4) between 15°N and 15°S (with a linear transition to 25°). The deep-sea circulation is not much affected by changes in the tropical SST and will not be described further.

The export production increases with the cooling of the tropical surface because of an increase of the density of the surface layer and hence an increased mixing with the nutrient-rich subsurface layers (in comparison with GFG, export production increases in GFGTC2 by 2% and in GFGTC4 by 4%; Figure 11c). Atmospheric pCO_2 is reduced by ~3 ppm in GFGTC2 and 6 ppm in GFGTC4 (Figure 11d) with an increase of solubility of CO_2 in colder seawater.

4.5. Sensitivity to Changes in the Wind Field

To investigate how glacial-interglacial changes in the wind field affect the deep-sea circulation, nutrients, and carbon isotopes, an experiment with glacial thermohaline boundary conditions but modern wind stress was carried out (experiment GFG Holocene Wind (GFGHW); Table 1). In the glacial Northern Hemisphere, stronger westerly wind with cool air temperatures causes an increase in the northward transport of the North Atlantic Current and promotes deep water formation. The increase of potential energy in the northern North Atlantic is balanced by an increase in potential energy in the Southern Ocean source, resulting in little net change in Atlantic overturning. The zonal wind stress in the southern West Wind Drift is increased by ~10% and can explain 1/3 of glacial-interglacial increase in the transport of the ACC through the Drake Passage (Table 2).

To separate the effect of Southern Ocean winds on the deep-sea circulation, in experiment GFG With Strong Southern Ocean Winds (GFGSW) the LGM wind stress was intensified in the zonal component by a factor of 1.5 in the region of the ACC (Figure 8 and Table 1). *Toggweiler and Samuels* [1993] (TS93) showed that an increase in the West Wind Drift τ_x in the Southern

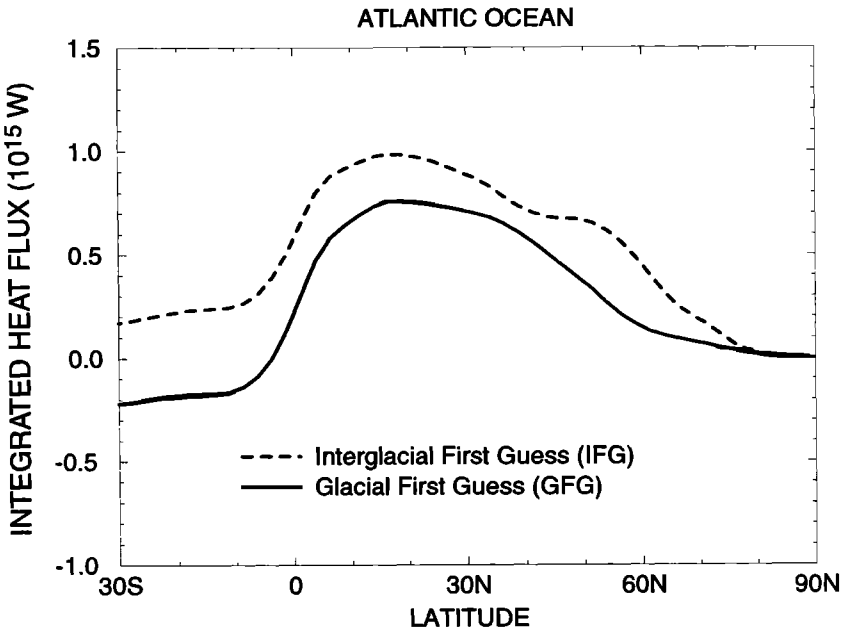

Figure 9. Zonally integrated transport of heat: OGCM response to present-day boundary conditions (IFG experiment, dashed) and to LGM boundary conditions (GFG experiment, solid).

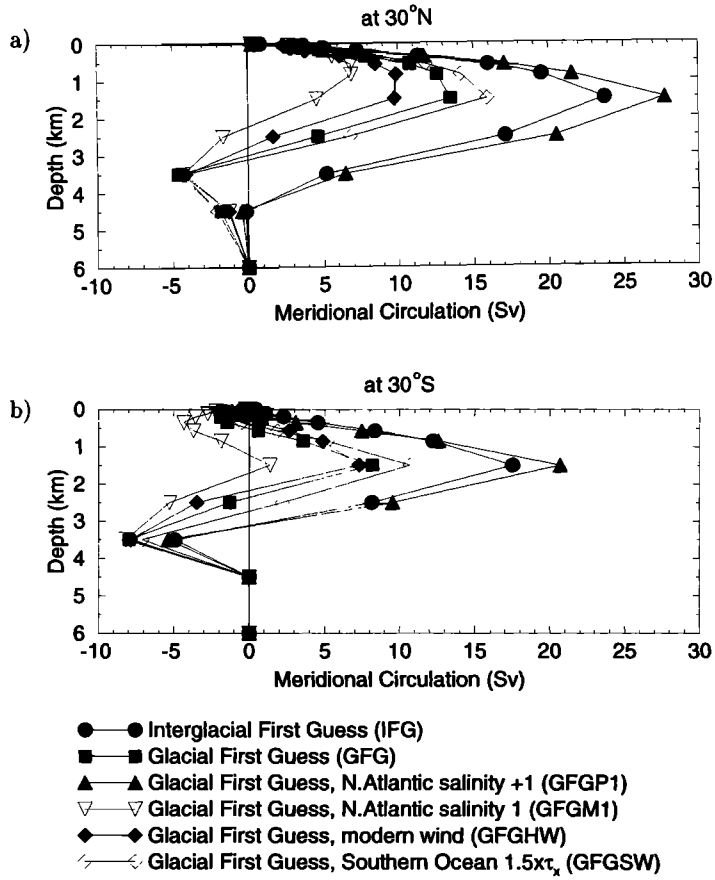

Figure 10. Zonally integrated flow in Sverdrup (Sv) accross (a) 30°N and (b) 30°S in the Atlantic for the seven experiments. Positive values denote a southward flow while negative values denote a northward flow (1 Sv = 10^6 m^3 s^{-1}).

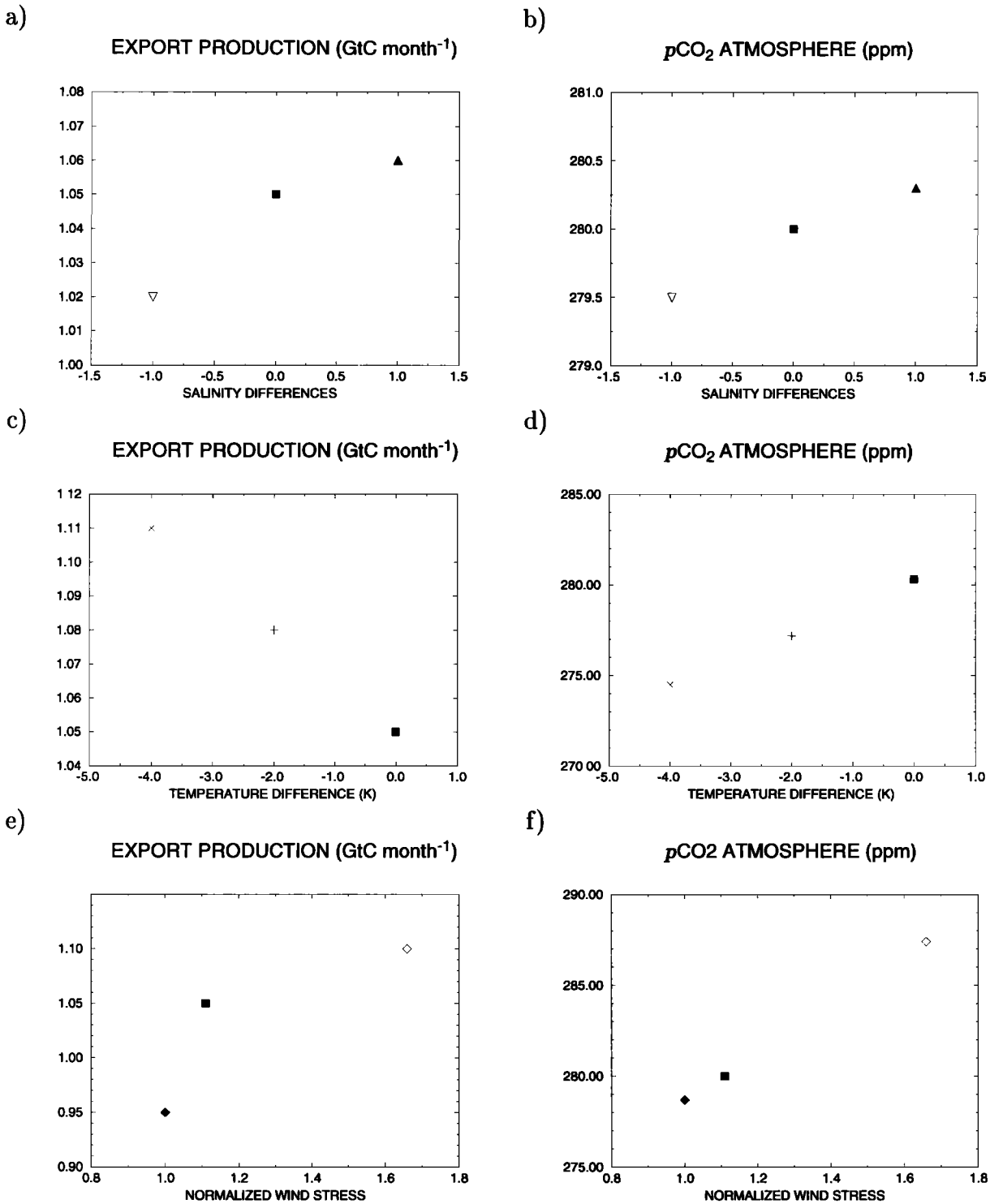

Figure 11. (a) and (b) Sensitivity of changes in export production and atmospheric pCO_2 due to changes in the prescribed surface salinity in the North Atlantic, (c) and (d) changes in the prescribed tropical 2 m air temperature, and (e) and (f) changes in the wind stress. Experiments are denoted by different signs: GFG, solid box; GFGM1, open triangle; GFGP1, solid triangle; GFTC2, plus; GFTC4, cross; GFGHW, open diamond; and GFGSW, solid diamond.

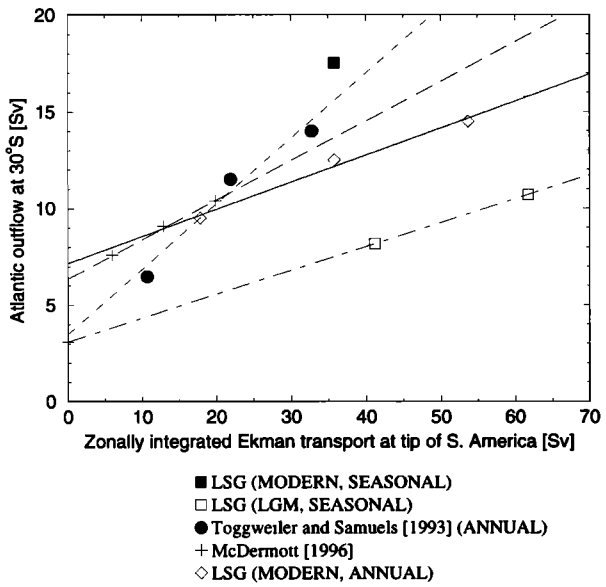

Figure 12. Outflow of the Atlantic Ocean at 30°S as a function of the zonally integrated Ekman transport T_E at the tip of South America (interglacial experiment IFG (solid boxes) and glacial experiments GFG (1,0 τ_x) and GFGSW (1,5 τ_x, open boxes)). For comparison, results of *Toggweiler and Samuels* [1993] (solid dots), of *McDermott* [1996](crosses), and experiments with an annual mean modern windfield (diamonds for 0.5, 1.0, and 1.5 τ_x) are shown. We note that the reference run of *Toggweiler and Samuels* [1993] is adjusted to the wind stess of *Hellerman and Rosenstein* [1983] (in zonally average about half as strong as ECHAM3/T42 wind stress in the Southern Ocean).

Ocean causes an increase in the Atlantic overturning circulation. The northward Ekman transport T_E at the latitude of the tip of South America can be defined according to the authors by

$$T_E = \int (-\tau_x/\rho_0 f)\, dx \qquad (8)$$

where ρ_0 denotes the reference density and f denotes the Coriolis parameter. Changes of the meridional transport at 30°S are of the order of the changes in the wind field. The comparably stronger simulated northward Ekman transport causes an increase of the North Atlantic Current with warm and saline surface water and an increase in the deepwater formation in the North Atlantic Ocean. This intensification of the North Atlantic Circulation, however, did not affect the deep sea temperature significantly. The relationship between the Ekman transport and the Atlantic deepwater is displayed in Figure 12. These results are also dependent on the formulation of the boundary conditions [*Rahmstorf and England*, 1997] and topography [*McDermott*, 1996]. By slowly varying wind fields in the Southern Ocean with a global coupled ocean-energy balance model, *Rahmstorf and England* [1997] achieve a much reduced wind stress dependence of the NCW outflow rates (for comparison, see *Rahmstorf and England* [1997, Figure 6]). Our model results indicate that the wind stress dependence of the NCW outflow rates is about half as strong as in experiments from TS93. The different outcomes of our simulation can be linked to the different formulations of energy dissipation in the interior of the model domains.

Changes in the wind field do not cause large changes in the distribution of phosphate and carbon isotopes in the deep sea (Figures 4e and 4f and 6e and 6f). Export production and atmospheric pCO_2 are in GFGSW with ~5% and 3% slightly higher than in GFG and GFGHW, respectively, because of a stronger mixing with the carbon-rich subsurface layers of the Southern Ocean (Figures 11e and 11f).

5. Summary and Conclusions

The following main conclusions can be outlined by our work.

1. A reasonable fit to deep-sea $\delta^{13}C$ and Cd/Ca data indicates a glacial North Component Water (NCW) flow, which is shallower and reduced by 50%, while the deep Atlantic is increasingly influenced by water masses from the Southern Ocean. In the Southern Ocean, glacial-interglacial changes in nutrients agree essentially with findings from Cd/Ca data and cannot explain the shift in $\delta^{13}C$. *LeGrand and Wunsch* [1995] estimated with an inverse multibox model that the Atlantic $\delta^{13}C$ distribution itself is inadequate to distinguish between the present-day circulation and a 50% reduction of NCW flow. The authors neglected geochemical processes, which might be critical to describe glacial-interglacial changes in carbon isotope and nutrient cycles [*Heinze et al.*, 1991; *Heinze and Hasselmann*, 1993; *Heinze and Broecker*, 1995; Archer et al., submitted manuscript, 1998]. Consideration of a possible *p*H effect, the Mackensen effect, as well as a probable increase in productivity by iron fertilization [*Broecker and Henderson*, 1998; Archer et al., submitted manuscript, 1998], indicates a need to include more complex biogeochemical processes. Thus more paleoceanographic tracers (e.g., Pa/Th [*Henderson et al.*, 1999; *Heinze et al.*, 1998]) should be used simultaneously to interpret the past ocean circulation.

2. Experiments to assess the sensitivity of the North Atlantic to the glacial circulation yield a wide spectrum of possible circulation patterns that cover the whole range from a super glacial Atlantic circulation, even stronger than at modern times, to an almost shutdown of the North Atlantic Deep Water source. These variations affect the biological pump as much as the $\delta^{13}C_{as}$. Changes in deep-sea $\delta^{13}C_{as}$ are of a similar magnitude to deviations between $\delta^{13}C$ in benthic foraminiferal shells and the $\delta^{13}C$ of DIC of their surrounding water masses.

3. Our model results show a much weaker relation between wind stress in the Southern Ocean and the Atlantic deep-sea circulation than the previous study of *Toggweiler and Samuels* [1993]. However, the results strongly depend on the way the models are parametrized (e.g., internal friction, choice of numerical scheme, boundary conditions [*Rahmstorf and England*, 1997], or topography [*McDermott*, 1996]).

4. All experiments with strongly varying boundary conditions and circulation patterns indicate that changes of the biological soft tissue pump have only little effect on changes in the atmospheric pCO_2. If the tropical surface is cooled by 4°C below the CLIMAP SST, a global reduction of the pCO_2 by 6 ppm is simulated. In high latitudes our results differ significantly from results of box models [e.g., *Wenk and Siegenthaler*, 1984], which show a high sensitivity of pCO_2 to the solubility pump. The sensitivity of atmospheric pCO_2 to high- and low-latitude forcing in GCMs differs generally from that found in box models. The difference is related to a much larger physical and geochemical parameter space in the former (e.g., GCMs have a much higher spatial resolution and consider nonlinear physical processes in high latitudes such as sea ice formation and convective overturning).

5. We suggest from our results the use of surface salinities as control variables for data assimilation experiments for an effective reduction of the paleonutrient model-data misfit.

Acknowledgments. We thank T. Crowley, C. Heinze, M. Lautenschlager, C. Winguth, and the reviewers for fruitful discussions. Also thanks go to J.-M. Campin, G. Hoffmann, E. Michel, S. Lorenz, M. Sarnthein, C. Schäfer-Neth, and M. Weinelt for having provided the data used in this study. J.-C. Duplessy is supported by CNRS, INSU (PNEDC), and CEA. This work was done at the MPI for Meteorology and at the University of Chicago (supported by Deutsche Forschungsgemeinschaft Grant DFG Ma 1070/2-1 and the Packard Foundation).

References

Altabet, M.A., Nitrogen and carbon isotopic tracers of the source and transformation of particles in the deep sea, in *Particle Flux in the Ocean*, *SCOPE*, vol. 57, edited by V. Ittekot et al., pp. 1-6, John Wiley, New York, 1996.

Arakawa, A., and V.R. Lamb, Computational design of the basic dynamical processes of the UCLA general circulation model, *Methods Comput. Phys., 16*, 173-283, 1977.

Barnola, J.M., D. Raynaud, Y.S. Korotkevich, and C. Lorius, Vostok ice core provides 160,000-year record of atmospheric CO_2, *Nature, 329*, 408-414, 1987.

Berger, W.H., K. Fischer, C. Lai, and G. Wu, Ocean productivity and organic carbon flux, *SIO Ref. 87-30*, Scripps Inst. of Oceanogr., La Jolla, Calif., 1987.

Bickert, T., and G. Wefer, Late quaternary deep water circulation in the South Atlantic: Reconstruction from carbonate dissolution and benthic stable isotopes, in *The South Atlantic*, edited by G. Wefer et al., pp. 559-620, Springer-Verlag, New York, 1996.

Boyle, E.A., Cadmium: Chemical tracer of deepwater paleoceanography, *Paleoceanography, 3*, 471-489, 1988.

Boyle, E.A., Cadmium and $\delta^{13}C$ paleochemical ocean distributions during stage 2 glacial maximum, *Annu. Rev. Earth Planet. Sci., 20*, 245-287, 1992.

Boyle, E.A., and L.D. Keigwin, North Atlantic thermohaline circulation during the past 20,000 years linked to high-latitude surface temperature, *Nature, 330*, 35-40, 1987.

Broecker, W.S., An oceanographic explanation for the apparent carbon isotope-cadmium discordancy in the glacial Antarctic, *Paleoceanography, 8*, 137-139, 1993.

Broecker, W.S., and G.M. Henderson, The sequence of events surrounding Termination II and their implications for the cause of glacial-interglacial CO_2 changes, *Paleoceanography, 13*, 352-364, 1998.

Broecker, W.S., and E. Maier-Reimer, The influence of air and sea exchange on the carbon isotope distribution in the sea, *Global Biogeochem. Cycles, 6*, 315-320, 1992.

Broecker, W.S., J.R. Ledwell, T. Takahashi, R. Weiss, L. Merlivat, L. Memery, T.-H. Peng, B. Jähne, and K.O. Münnich, Isotopic versus micrometeorologic ocean CO_2 fluxes: A serious conflict, *J. Geophys. Res., 91*, 10,517-10,527, 1986.

Broecker, W.S., M. Andree, G. Bonani, W. Wolfli, H. Oeschger, M. Clas, A. Mix, and W. Curry, Preliminary estimates for the radiocarbon age of deep water in the glacial ocean, *Paleoceanography, 3*, 659-669, 1988.

Bush, A.B., and S.G.H. Philander, The role of ocean-atmosphere interactions in tropical cooling during the Last Glacial Maximum, *Science, 297*, 1341-1344, 1998.

Climate: Long-Range Investigation, Mapping, and Prediction (CLIMAP) Project Members, Seasonal reconstruction of the the Earth's surface at the Last Glacial Maximum, *Geol. Soc. Am. Map Chart Ser., MC-36*, 1981.

Conkright, M.E., S. Levitus, and T.P. Boyer, *World Ocean Atlas 1994*, vol. 1, *Nutrients*, Nat. Oceanic and Atmos. Admin., Washington, D.C., 1994.

Crowley, T.J., Ice age terrestrial carbon changes revised, *Global Biogeochem. Cycles, 9*, 377-389, 1995.

Crowley, T.J., and S.K. Baum, Effect of vegetation on an ice-age climate model simulation, *J. Geophys. Res., 102*, 16,463-16,480, 1997.

Curry, W.B., and G.P. Lohmann, Reduced advection into Atlantic deep eastern basins during Last Glacial Maximum, *Nature, 306*, 577-580, 1983.

de Vernal, A., A. Rochon, C. Hillaire-Marcel, J-L.Turon, and J. Guiot, Quantitative reconstruction of sea surface conditions, seasonal extent of sea ice cover and meltwater discharges in high latitude marine environments from dinoflagellate cyst assemblages, in *Ice in the Climate System*, edited by W. Richard Peltier, pp. 11-621, Springer-Verlag, New York, 1993.

Duplessy, J.-C., N.J. Shackleton, R.G. Fairbanks, L.D. Labeyrie, D. Oppo, and N. Kallel, Deep water source variations during the last climatic cycle and their impact on the global deepwater circulation, *Paleoceanography, 3*, 343-360, 1988.

Duplessy, J.-C., L.D. Labeyrie, A. Juillet-Leclerc, F. Maitre, J. Dupart, and M. Sarnthein, Surface salinity reconstruction of the North Atlantic Ocean during the Last Glacial Maximum, *Oceanol. Acta, 14*, 311-324, 1991.

Duplessy, J.-C., L.D. Labeyrie, M. Paterne, S. Hovine, T. Fichefet, J. Duprat, and M. Labracherie, High latitude deep water sources during the Last Glacial Maximum and the intensity of the global oceanic circulation, in *The South Atlantic*, edited by G. Wefer et al., pp. 445-460, Springer-Verlag, New York, 1996.

Eppley, R., and B.T. Peterson, Particulate organic matter flux and planktonic new production in the deep ocean, *Nature, 282*, 677-680, 1979.

Fairbanks, R.G., A 17,000 year glacio-eustatic sea level record: Influence of glacial melting rates on the Younger Dryas event and deep-ocean circulation, *Nature, 143*, 637-642, 1989.

Fichefet, T., S. Hovine, and J.-C. Duplessy, A model study of the Atlantic thermohaline circulation during the Last Glacial Maximum, *Nature, 372*, 252-255, 1994.

Fieg, K., Der Ozean als Teil des gekoppelten Klimasystems: Versuch der Rekonstruktion der glazialen Zirkulation mit verschieden komplexen Atmosphärenkomponenten, *Ber. Polarforsch., 206*, Alfred-Wegener-Inst. für Polar- und Meeresforsch., Bremerhaven, Germany, 1996.

Francois, R., M.A. Altabet, E.-F. Yu, D.M. Sigman, M.P. Bacon, M. Frank, G. Bohrmann, G. Bareille, and L.D. Labeyrie, Contribution of Southern Ocean surface-water stratification to low atmospheric CO_2 concentration during the last glacial period, *Nature, 389*, 929-936, 1997.

Friedli, H., H. Loetscher, U. Siegenthaler, and B. Stauffer, Ice core records of $^{13}C/^{12}C$ record of atmospheric CO_2 in the past two centuries, *Nature, 324*, 237-238, 1986.

Ganopolski, A., S. Rahmstorf, V. Petoukhov, and M. Claussen, Simulation of modern and glacial climates with a coupled global model of intermediate complexity, *Nature, 391*, 351-356, 1998.

Guilderson, T.P., R.G. Fairbanks, and J.L. Rubenstone, Tropical temperature variations since 20,000 years ago: Modulating interhemispheric climate change, *Science, 263*, 663-665, 1994.

Hebbeln, D., T. Dokken, E.S. Anderson, M. Hald, and A. Elverthoi, Moisture supply for northern ice sheet growth during the Last Glacial Maximum, *Nature, 370*, 357-360, 1994.

Heinze, C., and W.S. Broecker, Closing off the Southern Ocean surface, *Paleoceanography, 10*, 49-58, 1995.

Heinze C., and K. Hasselmann, Inverse multiparameter modelling of paleoclimatic carbon cycle indices, *Quat. Res., 40*, 281-296, 1993.

Heinze, C., E. Maier-Reimer, and K. Winn, Glacial pCO_2 reduction by the World Ocean: Experiments with the Hamburg carbon cycle model, *Paleoceanography, 6*, 395-430, 1991.

Heinze, C., E. Maier-Reimer, A. Winguth, and D. Archer, A global oceanic sediment model for longterm climate studies, *Rep. 248*, Max-Planck-Inst. für Meteorol., Hamburg, Germany, 1998.

Hellerman, S., and M. Rosenstein, Normal monthly wind stress over the world ocean with error estimates, *J. Phys. Oceanogr., 13*, 1093-1104, 1983.

Henderson, G.M., C. Heinze, R. Anderson, and A. Winguth, Global distribution of the ^{230}Th flux to ocean sediments constrained by GCM modelling, *Deep-Sea Res.*, in press, 1999.

Herterich K., et al., Reconstructing and modelling the Last Glacial Maximum: Beyond CLIMAP, in *Proxies in Paleoceanography*, edited by G. Wefer and G.F. Fischer, Springer-Verlag, New York, in press, 1999.

Honjo, S., S.J. Manganini, and J. Cole, Sedimentation of biogenic matter in the deep ocean, *Deep Sea Res., Part A, 29*, 609-625, 1982.

Keigwin, L.D., G.A. Jones, and P.N. Froehlich, A 15,000 year paleoenvironmental record from Meiji Seamount, far northwest Pacific, *Earth Planet. Sci. Lett.*, 111, 425-440, 1992.

Kellog, T.B., Paleoclimatology and paleooceanography of the Norwegian and Greenland Seas: Glacial-interglacial contrasts, *Boreas, 9*, 5-37, 1980.

Klinck, J.M., and D.A. Smith, Effect of wind changes during the Last Glacial Maximum on the circulation in the Southern Ocean, *Paleoceanography, 8*, 427-433, 1993.

Kroopnick, P.M., The distribution of $\delta^{13}C$ of ΣCO_2 in the world oceans, *Deep Sea Res. Part A, 32*, 57-84, 1985.

Labeyrie, L.D., J.-C. Duplessy, J. Dupart, A. Juillet-Leclerc, J. Moyes, E. Michel, N. Kallel, and N.J. Shackleton, Changes in the vertical structure of the North Atlantic Ocean between glacial and modern times, *Quat. Sci. Rev., 11*, 401-413, 1992.

Lautenschlager, M., U. Mikolajewicz, E. Maier-Reimer, and C. Heinze, Application of ocean models for the interpretation of atmospheric general circulation model experiments on the climate of the Last Glacial Maximum, *Paleoceanography, 7*, 769-782, 1992.

LeGrand, P., and C. Wunsch, Constraints from paleotracer data on the North Atlantic circulation during the Last Glacial Maximum, *Paleoceanography, 10*, 1011-1045, 1995.

Levitus, S., *Climatological Atlas of the World Ocean, Prof. Pap. 13*, Nat. Oceanic and Atmos. Admin., Rockville, Md., 1982.

Lorenz, S., B. Grieger, P. Helbig, and K. Herterich, Investigating the sensitivity of the atmospheric general circulation model ECHAM 3 to paleoclimatic boundary conditions, *Geol. Rundsch., 85*, 513-524, 1996.

Lynch-Stieglitz, J., and R.G. Fairbanks, A conservative tracer for glacial ocean circulation from carbon isotope and paleonutrient measurements in benthic foraminifera, *Nature, 369*, 308-310, 1994.

Lynch-Stieglitz, J., T.F. Stocker, W.S. Broecker, and R.G. Fairbanks, The influence of air-sea exchange on the isotopic composition of oceanic carbon: Observations and modeling, *Global Biogeochem. Cycles, 9*, 653-665, 1995.

Mackensen, A., Foraminiferen und Paläoozeanographie hoher Breiten, *Ber. Polarforsch., 243*, Alfred-Wegener-Inst. für Polar- und Meeresforsch., Bremerhaven, Germany, 1997.

Mackensen, A., H.-W. Hubberten, T. Bickert, G. Fischer, and D.K. Fütterer, The $\delta^{13}C$ in benthic foraminiferal tests of *Fontbotia wuellerstorfi* (Schwager) relative to the $\delta^{13}C$ of dissolved inorganic carbon in Southern Ocean Deep Water: Implications for glacial ocean circulation models, *Paleoceanography, 8*, 587-610, 1993.

Maier-Reimer, E., Geochemical cycles in an ocean general circulation model: Preindustrial tracer distributions, *Global Biogeochem. Cycles, 7*, 645-677, 1993.

Maier-Reimer, E., and K. Hasselmann, Transport and storage of CO_2 in the ocean: An inorganic ocean-circulation carbon cycle model, *Clim. Dyn., 2*, 63-90, 1987.

Maier-Reimer, E., U. Mikolajewicz, and K. Hasselmann, Mean circulation of the Hamburg LSG OGCM and its sensitivity to the thermohaline surface forcing, *J. Phys. Oceanogr., 23*, 731-757, 1993.

Maier-Reimer, E., U. Mikolajewicz, and A. Winguth, Interactions between ocean circulation and the biological pumps in the global warming, *Clim. Dyn., 12*, 711-721, 1996.

McCorkle, D.C., and L.D. Keigwin, Depth profile of $\delta^{13}C$ in bottom water and core top *C. wuellerstorfi* on the Ontong Java Plateau and Emperor Seamounts, *Paleoceanography, 9*, 197-208, 1994.

McDermott, D.A., The regulation of northern overturning by Southern Hemisphere winds, *J. Phys. Oceanogr., 26*, 1234-1255, 1996.

Michel, E., L.D. Labeyrie, J.-C. Duplessy, and N. Gorfi, Could deep Subanarctic convection feed the world deep basins during the Last Glacial Maximum?, *Paleoceanography, 10*, 927-942, 1995.

Mikolajewicz, U., A meltwater induced collapse of the "conveyor belt" thermohaline circulation and its influence on the distribution of $\Delta^{14}C$ and $\delta^{18}O$ in the oceans, *Rep. 189*, Max-Planck-Inst. für Meteorol., Hamburg, Germany, 1996.

Mikolajewicz, U., E. Maier-Reimer, T.J. Crowley, and K.-Y. Kim, Effect of Drake and Panamanian gateways on the circulation of an ocean model, *Paleoceanography, 8*, 409-426, 1993.

Mook, W.G., J.C. Bommerson, and W.H. Staverman, Carbonate isotope fraction between dissolved bicarbonate and gaseous carbon dioxide, *Earth Planet. Sci. Lett., 22*, 169-176, 1974.

Najjar, R.G., J.L. Sarmiento, and J.R. Toggweiler, Downward transport and fate of organic matter in the ocean: Simulations with a general circulation

model, *Global Biogeochem. Cycles, 6*, 45-76, 1992.

Östlund, H.G., C. Craig, W.S. Broecker, and D. Spencer, *GEOSECS Atlantic, Pacific and Indian Ocean Expeditions: Shorebased Data and Graphics*, GEOSECS Atlas Ser., vol. 7, 200 pp., U.S. Gov. Print. Off., Washington, D.C., 1987.

Rahmstorf, S., and M. England, Influence of Southern Hemisphere winds on North Atlantic Deep Water flow, *J. Phys. Oceanogr., 27*, 2040-2054, 1997.

Rau, G.H., T. Takahashi, D.J. Des Marais, and C.W. Sullivan, Particulate organic matter $\delta^{13}C$ variations across the Drake Passage, *J. Geophys. Res., 96*, 15,131-15,136, 1991.

Rind, D., and D. Peteet, Terrestrial conditions at the Last Glacial Maximum and CLIMAP sea-surface temperature estimates: Are they consistent?, *Quat. Res., 24*, 1-22, 1985.

Rosell-Melé, A., and N. Koc, Paleoclimatic significance of the stratigraphic occurence of photosynthetic biomarker pigments in the Nordic Seas, *Geology, 25*, 49-52, 1997.

Sanyal, A., N.G. Hemming, G.N. Hanson, and W.S. Broecker, Evidence for a higher pH in the glacial ocean from boron isotopes in foraminifera, *Nature, 373*, 234-236, 1995.

Sarnthein, M., K. Winn, S.J.A. Jung, J.-C. Duplessy, L. Labeyrie, H. Erlenkeuser, and G. Ganssen, Changes in east Atlantic deepwater circulation over the last 30,000 years: Eight time slice reconstructions, *Paleoceanography, 9*, 209-267, 1994.

Sarnthein, M., et al., Variations in Atlantic surface ocean paleoceanography, 50°-80°N: A time-slice record of the last 30,000 years, *Paleoceanography, 10*, 1063-1094, 1995.

Schäfer-Neth, C., Modellierung der Paläoozeanographie des nördlichen Nordatlantiks zur letzten Maximalvereisung, *Ber. 51*, Sonderforschungsbereich 313, Christian-Albrechts-Univ. zu Kiel, Kiel, Germany, 1994.

Seidov, D., and B.J. Haupt, Global ocean thermohaline conveyor at present and in the late Quaternary, *Geophys. Res. Lett., 24*, 2817-2820, 1997.

Seidov, D., M. Sarnthein, K. Stattegger, R. Prien, and M. Weinelt, North Atlantic ocean circulation during the Last Glacial Maximum and subsequent meltwater event: A numerical model, *J. Geophys. Res., 101*, 16,305-16,332, 1996.

Shackleton, N.J., J.-C. Duplessy, M. Arnold, P. Maurice, M.A. Hall, and J. Cartlidge, Radiocarbon age of last glacial Pacific deep water, *Nature, 335*, 708-711, 1988.

Siegenthaler, U., and K.O. Münnich, $^{13}C/^{14}C$ fractionation during CO_2 transfer from air to sea, in *Carbon Cycle Modelling, SCOPE*, vol. 16, edited by B. Bolin, pp. 249-258, John Wiley, New York, 1981.

Sikes, E.L., and L.D. Keigwin, Equatorial Atlantic sea surface temperature for the last 30 kyr: A comparison of $U^{k'}_{37}$, $\delta^{18}O$ and foraminiferal assemblage temperature estimates, *Paleoceanography, 9*, 31-45, 1994.

Spero, H.J., J. Bijma, D.W. Lea, and B. Bemis, Effect of seawater carbonate concentrations on foraminiferal carbon and oxygen isotopes, *Nature, 390*, 497-500, 1997.

Stocker, T.F., A glimpse of the glacial, *Nature, 391*, 338-339, 1998.

Stommel, H., and A.B. Arons, On the abyssal circulation of the World Ocean, II, An idealized model of the circulation pattern and amplitude in oceanic basins, *Deep Sea Res., 6*, 217-233, 1960.

Stute, M., M. Forster, H. Frischkorn, A. Serejo, J.F. Clark, P. Schlosser, W. Broecker, and G. Bonani, Cooling of tropical Brazil (5°) during the Last Glacial Maximum, *Science, 269*, 379-383, 1995.

Takahashi, T., W.S. Broecker, and S. Langer, Redfield ratio based on chemical data from isopycnal surfaces, *J. Geophys. Res., 90*, 6907-6924, 1985.

Toggweiler, J.R., and B. Samuels, Is the magnitude of the deep outflow from the Atlantic Ocean actually governed by Southern Hemisphere winds?, in *The Global Carbon Cycle, NATO ASI Ser.*, vol. I15, edited by M. Heimann, pp. 303-331, Springer-Verlag, New York, 1993.

Vogel, J.G., P.M. Grootes, and W.G. Mook, Isotopic fractionation beween gaseous and dissolved carbon dioxide, *Z. Phys., 230*, 225-238, 1970.

Volk, T., and M.I. Hoffert, Ocean carbon pumps: Analysis of relative strengths and efficiencies in ocean-driven atmospheric CO_2 changes, in *The Carbon Cycle and Atmospheric CO_2: Natural Variations Archean to Present, Geophys. Monogr. Ser.*, vol. 32, edited by E.T. Sunquist and W.S. Broecker, pp. 99-110, AGU, Washington, D.C., 1985.

Weaver, A.J., M. Eby, A.F. Fanning, and E.C. Wiebe, Simulated influence of carbon dioxide, orbital forcing and ice sheets on the climate of the Last Glacial Maximum, *Nature, 394*, 847-853, 1998.

Webb, R.S., D.H. Rind, S.J. Lehman, R.J. Healy, and D. Sigman, Influence of ocean heat transport on the climate of the Last Glacial Maximum, *Nature, 385*, 695-699, 1997.

Weinelt, M., M. Sarnthein, U. Pflaumann, H. Schulz, J. Jung, and H. Erlenkeuser, Ice-free Nordic Seas during the Last Glacial Maximum? Potential sites of deepwater formation, *Paleoclimates, 1*, 283-309, 1996.

Weiss, R.F., Carbon dioxide in water and seawater: The solubility of a non ideal gas, *Mar. Chem., 2*, 203-215, 1974.

Wenk, T., and U. Siegenthaler, The high-latitude ocean as a control of atmospheric CO_2, in *The Carbon Cycle and Atmospheric CO_2: Natural Variations Archean to Present, Geophys. Monogr. Ser.*, vol. 32, edited by E.T. Sunquist and W.S. Broecker, pp. 185-194, AGU, Washington, D. C., 1985.

Winguth, A.M.E., Assimilation von $\delta^{13}C$-Daten aus marinen Sedimentbohrkernen in das LSG zur Rekonstruktion der Ozeanzirkulation während des letzten glazialen Maximums, *Examensarbeit 47*, Max-Planck-Inst. für Meteorol., Hamburg, Germany, 1997.

Winguth, A.M.E., M. Heimann, K. D. Kurz, E. Maier-Reimer, U. Mikolajewicz, and J. Segschneider, El Niño-Southern Oscillation related fluctuations of the marine carbon cycle, *Global Biogeochem. Cycles, 8*, 39-63, 1994.

Winguth, A.M.E., D. Archer, E. Maier-Reimer, and U. Mikolajewicz, Paleonutrient data analysis of the glacial Atlantic using an adjoint ocean general circulation model, *Rep. 281*, Max-Planck-Inst. für Meteorol., Hamburg, Germany, 1998.

Woodruff, S.D., R.J. Slutz, R.L. Jenne, and P.M. Steurer, A comprehensive ocean-atmosphere data set, *Bull. Am. Meteorol. Soc., 68*, 1239-1250, 1987.

Yu, E.-F., R. Francois, and M.P. Bacon, Similar rates of modern and last-glacial ocean thermohaline circulation inferred from radiochemical data, *Nature, 379*, 689-694, 1996.

Zahn, R., and A.C. Mix, Benthic foraminiferal $\delta^{18}O$ in the ocean's temperature-salinity-density field: Constraints on ice age thermohaline circulation, *Paleoceanography, 6*, 1-20, 1991.

D. Archer and A. M. E. Winguth, Department of Geophysical Sciences, University of Chicago, Chicago, IL 60637. (e-mail: winguth@starbuck.uchicago.edu)

Jean-Claude Duplessy, Centre des Faibles Radioactivites, Laboratoire mixte CNRS-CEA, F-91198 Gif sur Yvette cedex, France.

E. Maier-Reimer and U. Mikolajewicz, Max-Planck-Institut für Meteorologie, D-20146 Hamburg, Germany.

(Received July 22, 1998;
revised December 7, 1998;
accepted January 4, 1999.)